The Abdus Salam International Centre for Theoretical Physics

Oct 26, 2017

Nonlinear electrodynamics in Weyl semimetals: Floquet bands and photocurrent generation

Ching-Kit Chan

University of California Los Angeles

Theory

Patrick Lee *(MIT)*

Experiment

Su-Yang Xu, F. Mahmood, Nuh Gedik *(MIT)*

Qiong Ma, Pablo Jarillo-Herrero *(MIT)*

Outline

Nonequilibrium physics: light + topological matter + dynamics

▪ Floquet-Bloch bands in gapless topological materials

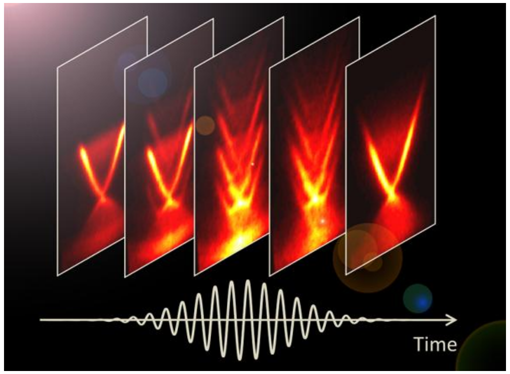

- Mahmood, CKC, et. al., Nature Physics, 2016
- CKC, Lee, et. al., PRL, 2016
- CKC, Oh, Han and Lee, PRB, 2016

▪ Photocurrent in Weyl semimetals

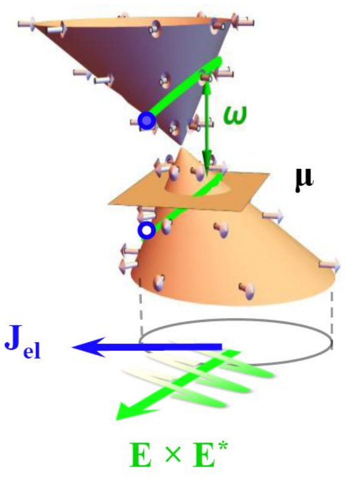

- CKC, Lindner, Refael and Lee, PRB, 2017
- Ma, Xu, CKC, et. al. Nature Physics, 2017

Example of driven system: Kapitza Pendulum

New physics can emerge when physical systems are driven far away from equilibrium

(https://www.youtube.com/watch?v=rwGAzy0noU0)

Motivation – Nonequilibrium Floquet bands

	<u>Equilibrium</u> [H]	**<u>Nonequilibrium</u> [H(t)=H(t+T)]**
Evolution:	$U(t) = e^{-iHt}$	$U(t,0) = e^{-i\int_0^t dt' H(t')}$
Eigenenergies and eigenstates:	$U(t)\|n\rangle = e^{-iE_n t}\|n\rangle$	$U(T,0)\|n_F\rangle = e^{-iE_{F,n}T}\|n_F\rangle$
		?
State evolution:	$\|\psi(t)\rangle = \sum_n \langle n\|\psi(0)\rangle \|n(t)\rangle$	$\|\psi(t,0)\rangle = \sum_n \langle n_F\|\psi(0)\rangle \|n_F(t)\rangle$

“Floquet-wave”:

$$|n_F(t)\rangle = e^{-iE_n t}|p_n(t)\rangle$$

$$|p_n(t)\rangle = |p_n(t+T)\rangle$$

Well-defined quasi-Hamiltonian in periodically driven systems

Motivation – Floquet-Bloch bands

- Spatial periodicity in lattice
  → Bloch bands

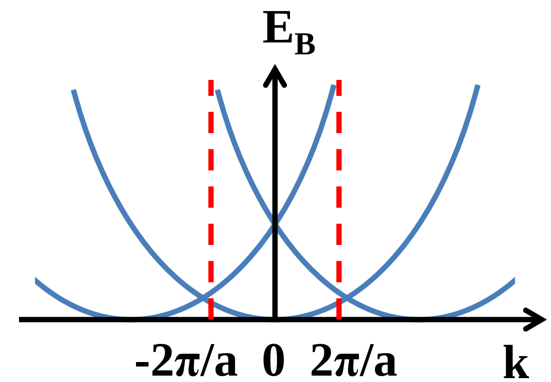

$$\boxed{\psi_B(r) = e^{ikr}u(r)} \quad u(r) = u(r+R)$$

- Temporal periodicity due to laser drives
  → Floquet bands

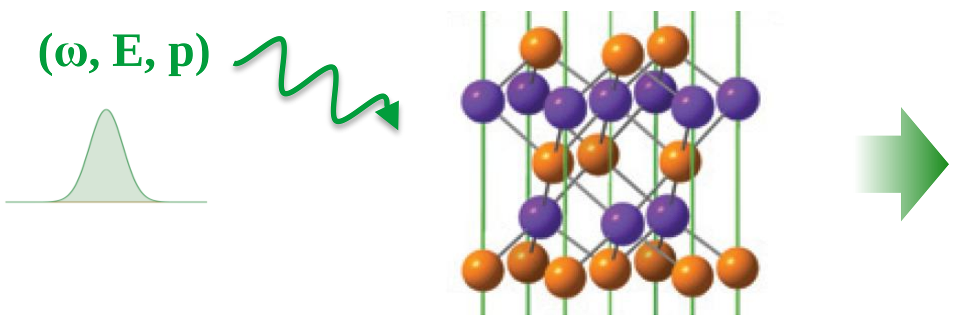

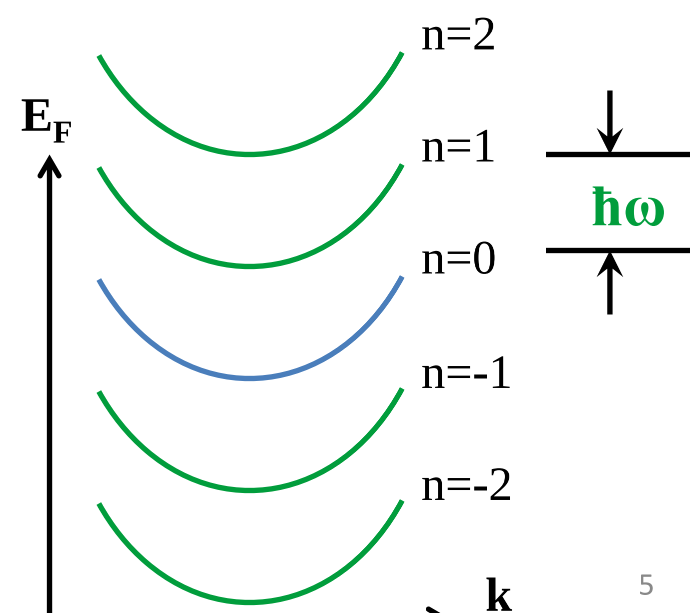

$$\boxed{\psi_F(t) = e^{-iE_Ft}p(t)} \quad p(t) = p(t+T)$$

Motivation – Floquet topological insulator

Light induced topological matter (Lindner, Refael and Galitski, 2011)

Ordinary insulator

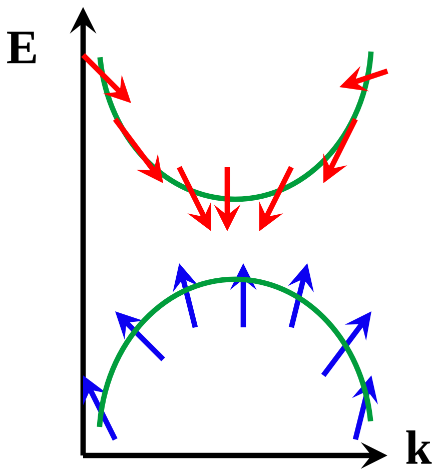

Laser drive

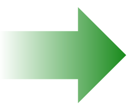

Photoinduced band inversion

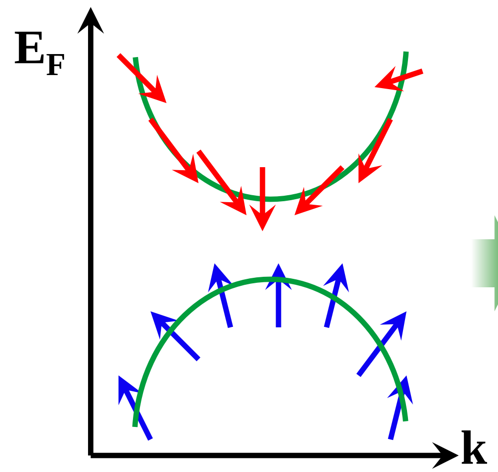

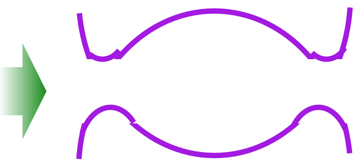

Nontrivial Floquet band

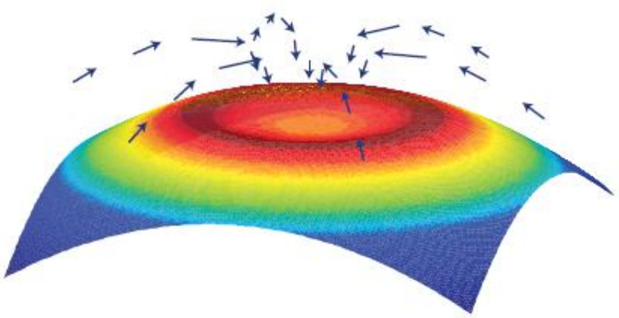

Tuning topology by light!

Many new questions to be explored

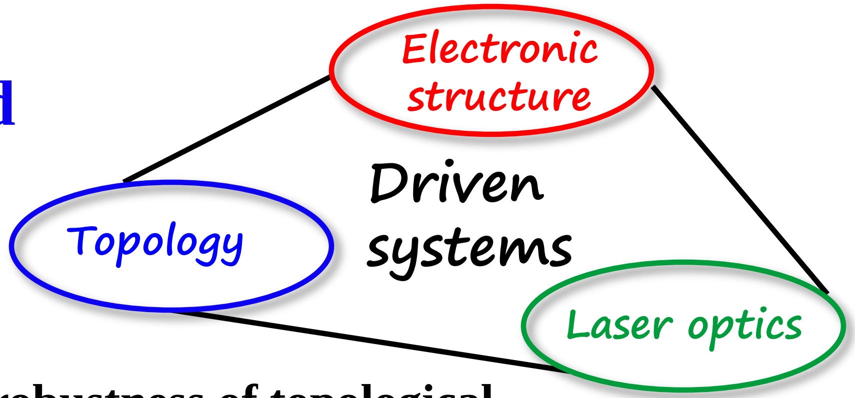

-Floquet-band manipulation

- Interplay between intense laser drive and robustness of topological materials (e.g. 2D Dirac, 3D Dirac or Weyl semimetals)

- Roles of symmetry

-Topological phase transitions

- Experimental relevance: photoemission, photoinduced transport phenomena, optical responses, etc.

-And more:

- Dynamics/evolution
- Dissipation
- Heating
- Disorder
- Strong correlation

Driven 2D Massless Dirac Fermions

- 2D Floquet-Bloch bands
- Time-resolved ARPES
- New experiment+theory findings

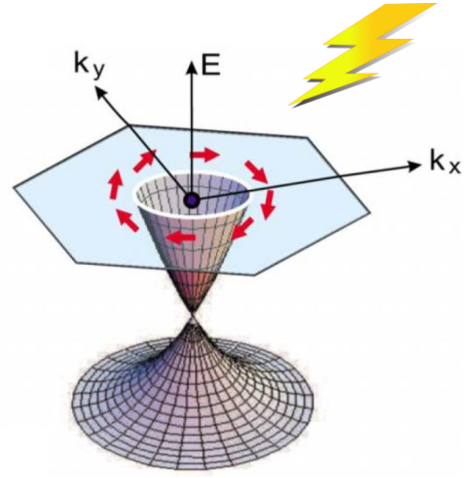

Driving the surface of 3D topological insulator

Linearly polarized drive:

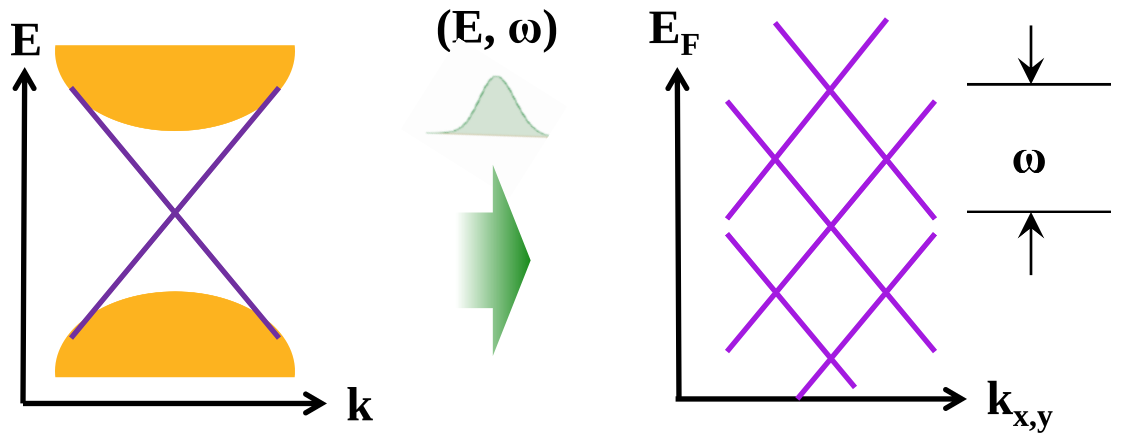

2D Dirac surface state **Replica of Floquet-Dirac band**

Circularly polarized drive:

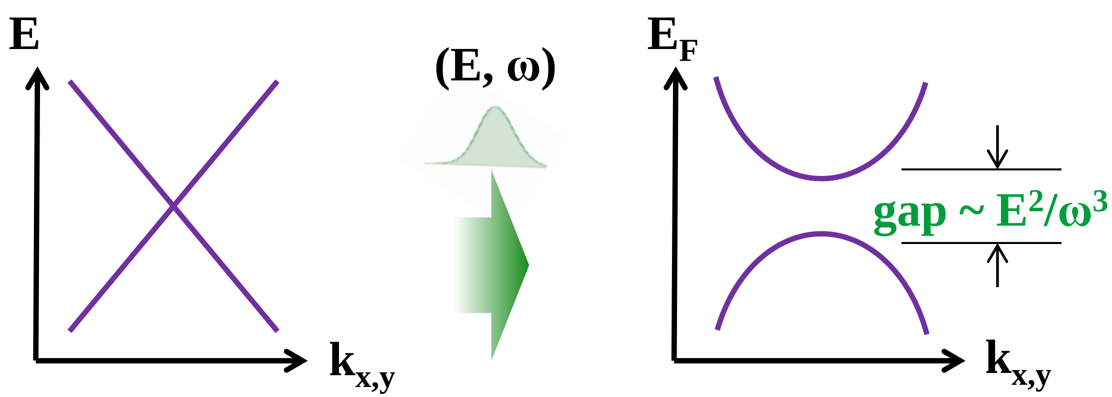

Light induced band gap due to broken time-reversal symmetry

Magnus expansion: $$H_F = H_0 + \frac{1}{\omega}\sum_n \frac{1}{n}[H_{-n}, H_n] + O\left[\frac{1}{\omega^2}\right]$$

Experimental advance in Time-Resolved ARPES

Pump-probe measurement of photoexcited electron (k, E, t):

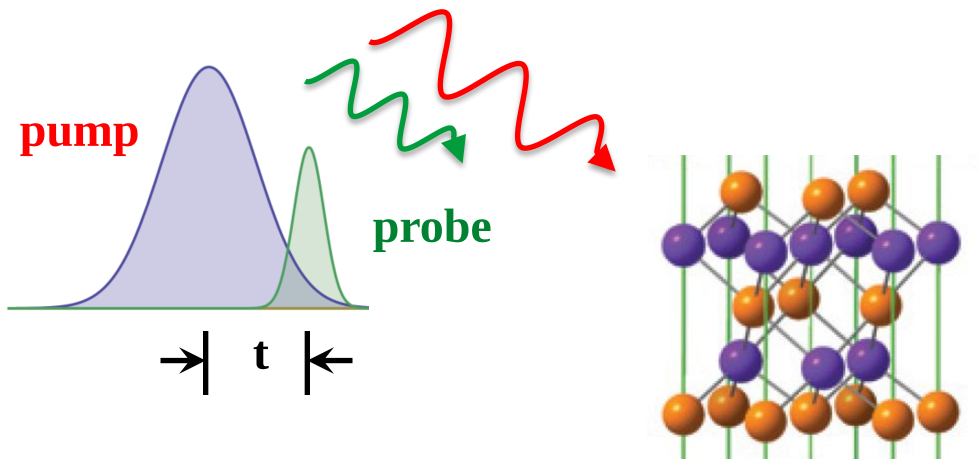

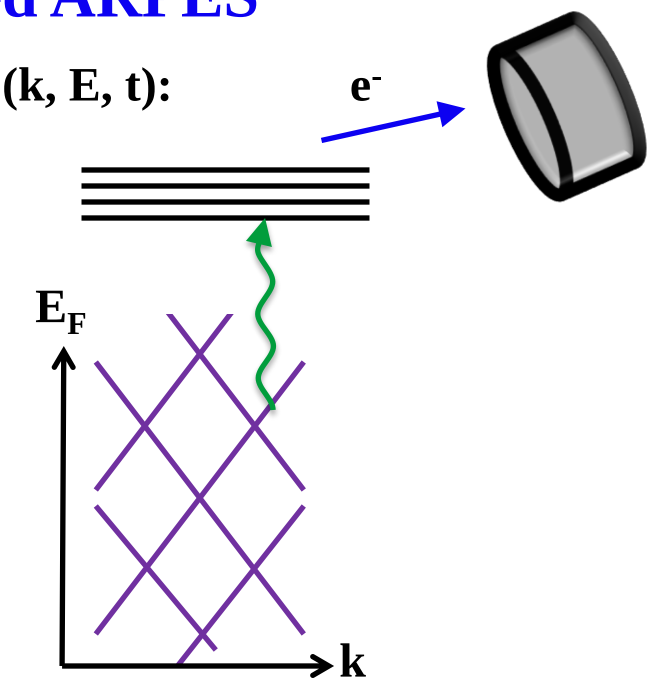

Experiment in Gedik's group @ MIT:

Sub-pico second laser pulse driving 3D TI Bi_2Se_3

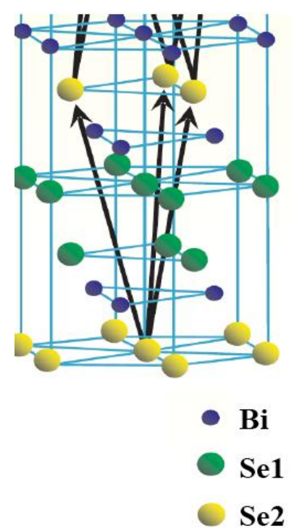

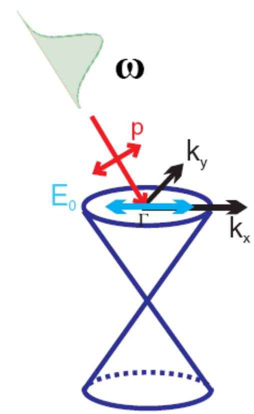

Floquet-Bloch band on the surface of topological insulator

Floquet-Bloch bands by driving the surface of Bi_2Se_3

(F. Mahmood, CKC, et. al., Nature Physics, 2016)

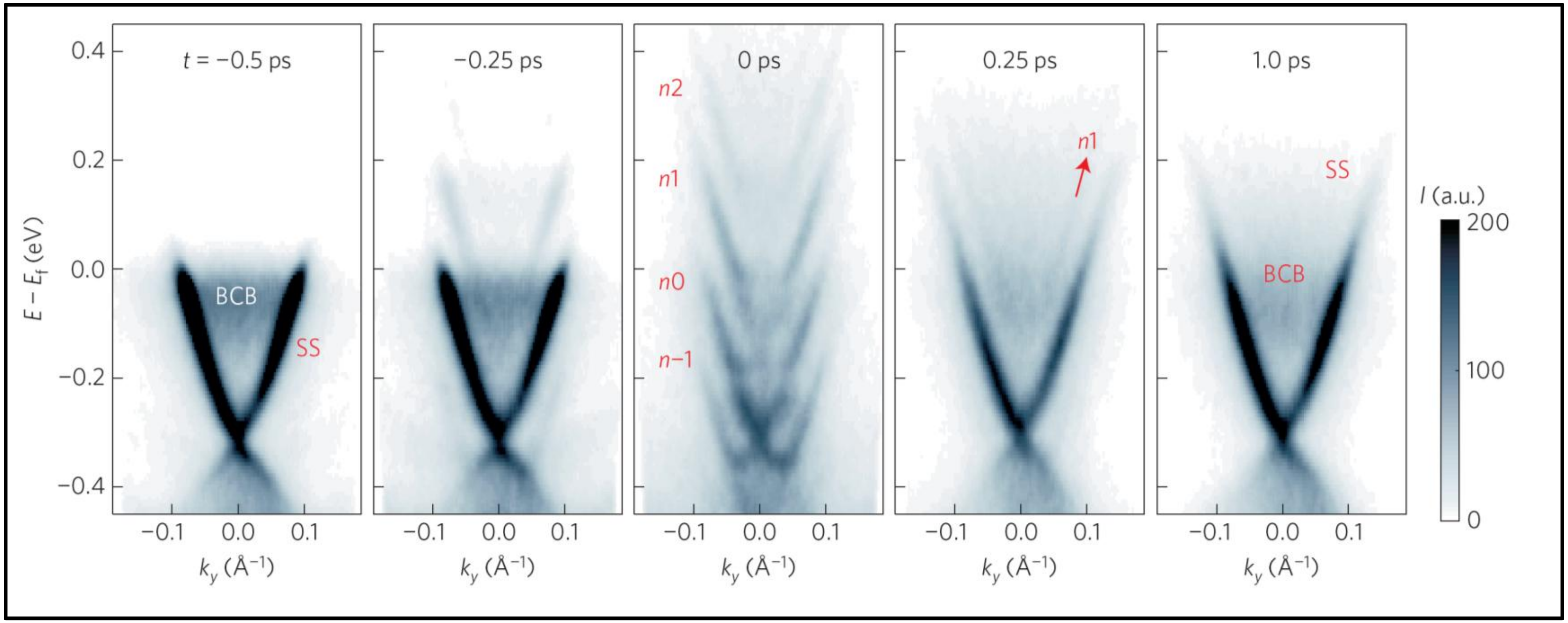

- CO_2 laser: ħω ~ 120 meV
- Gap ~ 60 meV, match well with theory

- **Spectral weight discrepancy**

Interference between Floquet and Volkov effects

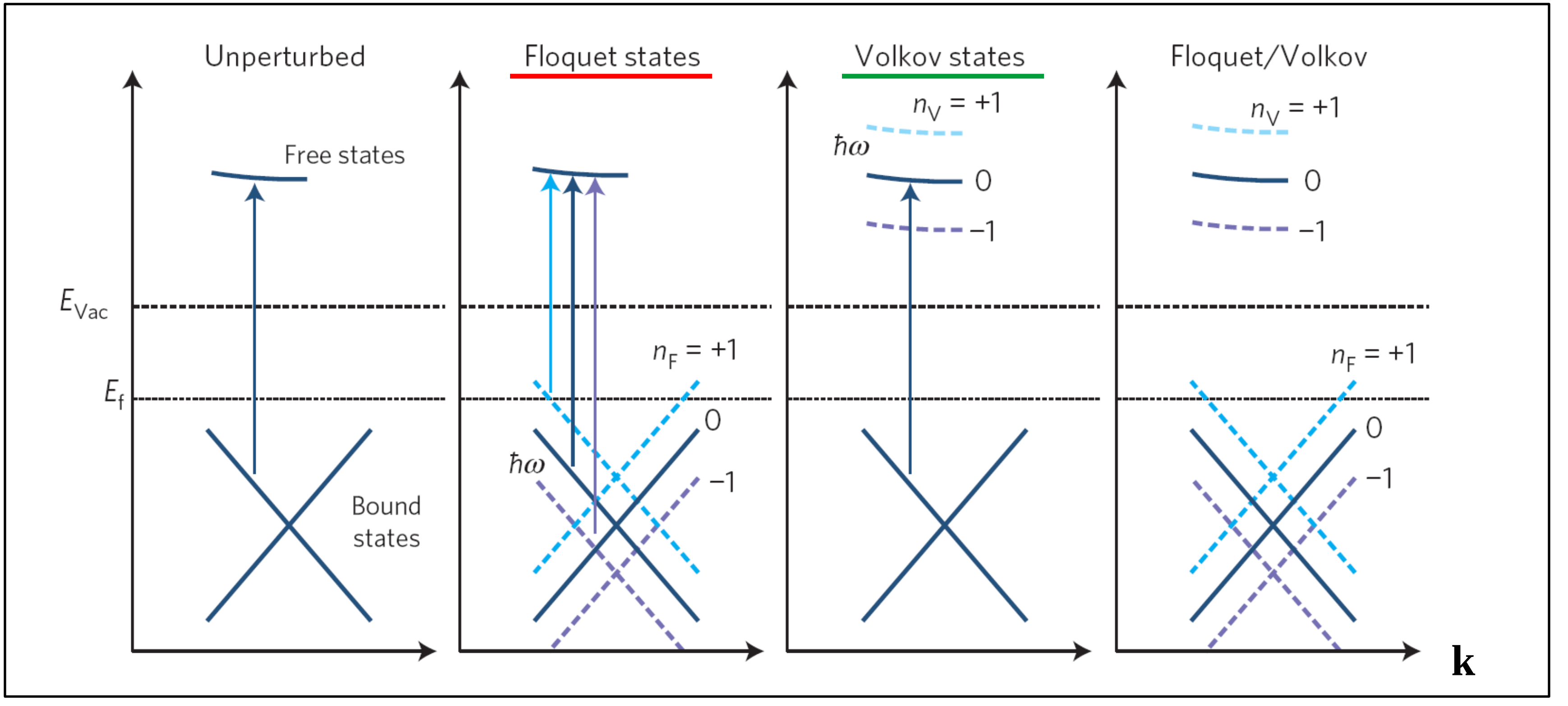

$$I(\vec{k},E) \sim \int_{t_i}^{t_f} dt \int_0^{t_f - t} d\tau\, s(t)\, s(t+\tau) \underline{\sum_{\sigma_1,\sigma_2,\sigma_f} M_k^*(\sigma_f,\sigma_1) M_k(\sigma_f,\sigma_2)}$$ spin-probe effect

$$\text{x}\;\; 2\,\mathrm{Re}\left[\underline{G^{<}_{k,\sigma_1,\sigma_2}(t,\tau)}\; e^{-iE\tau/\hbar}\right] \underline{e^{-i\int_t^{t+\tau} dt' H_{\mathrm{LAPE}}(t')/\hbar}}$$

Floquet **Volkov**

Spectral weights analysis

P-polarized pump:

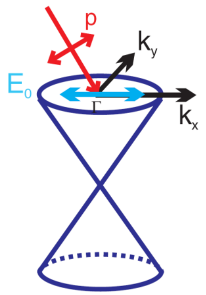

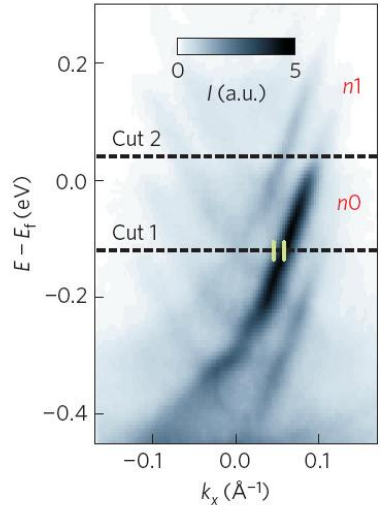

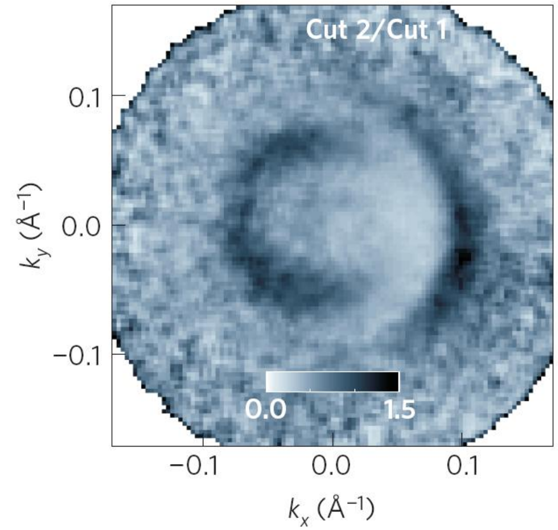

(No fitting parameters)

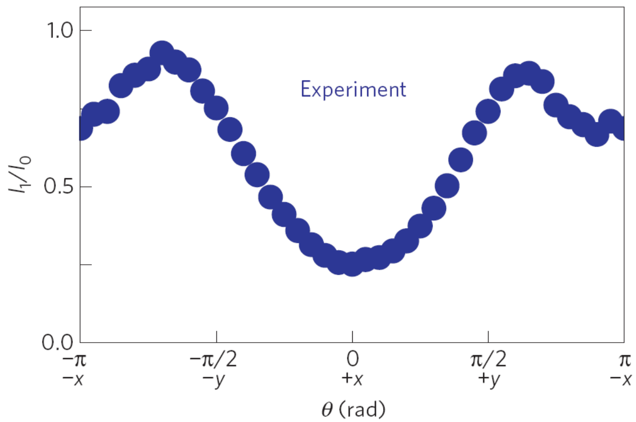

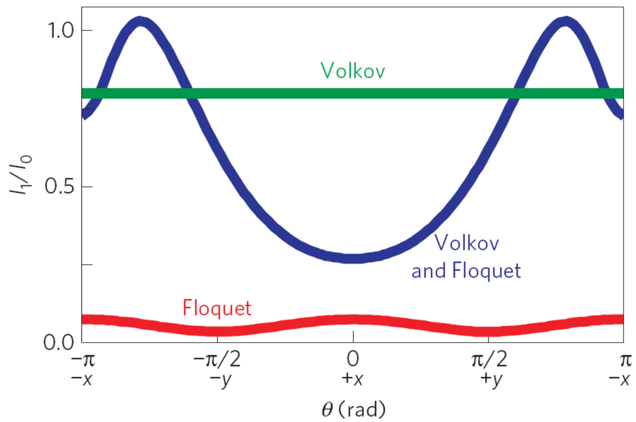

(F. Mahmood, CKC, et. al., Nature Physics, 2016)

More spectral weight analysis

P-polarized pump:

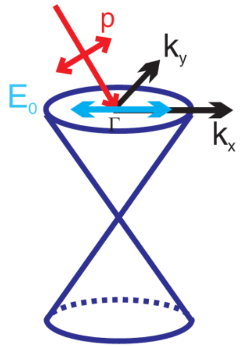

Higher order Floquet bands

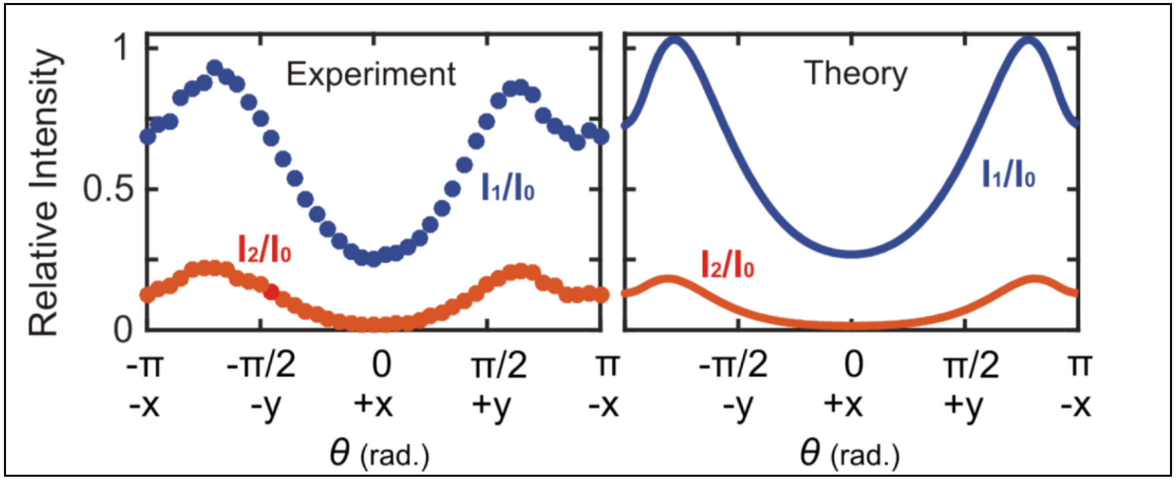

Purely intrinsic Floquet band using S-polarized pump

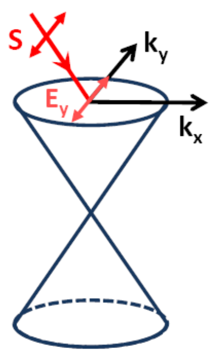

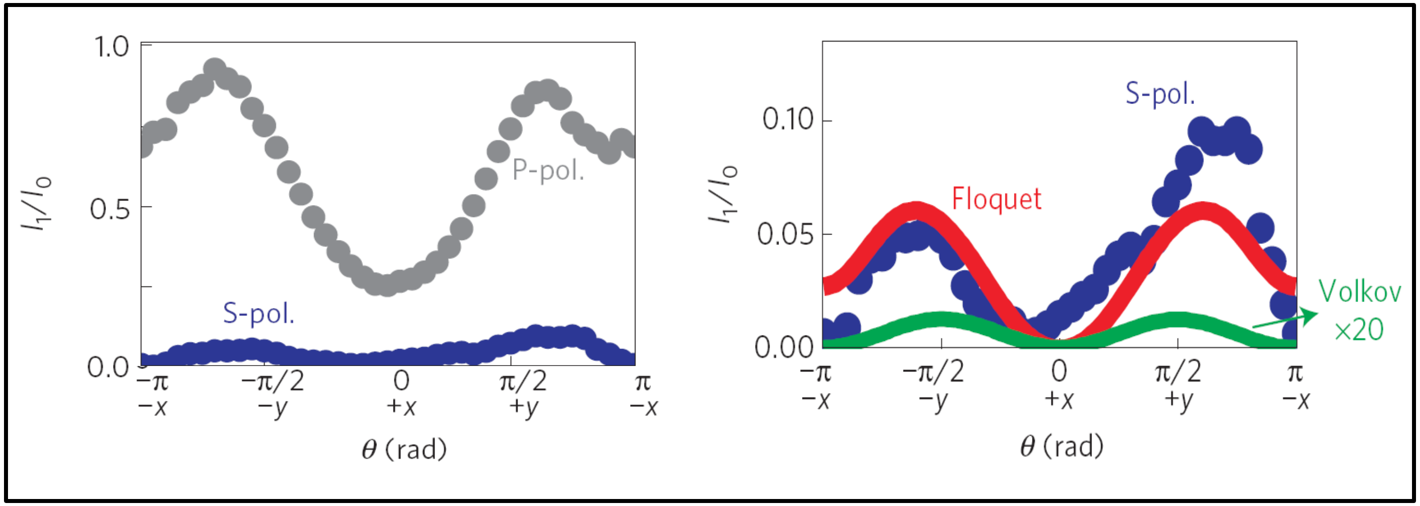

Summary (what we learnt…)

- Driving 2D Dirac generates Floquet bands and tunable gaps controlled by laser polarization, frequency and intensity through TR breaking

- Spectral weights are quantitatively understood in terms of intrinsic and extrinsic Floquet effects

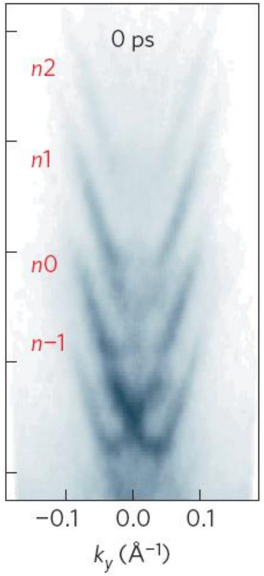

- An excellent moment for more exotic ideas!

Driven 3D Weyl Semimetals

- Role of chirality
- Photoinduced anomalous Hall effect
- Semimetal transitions by light

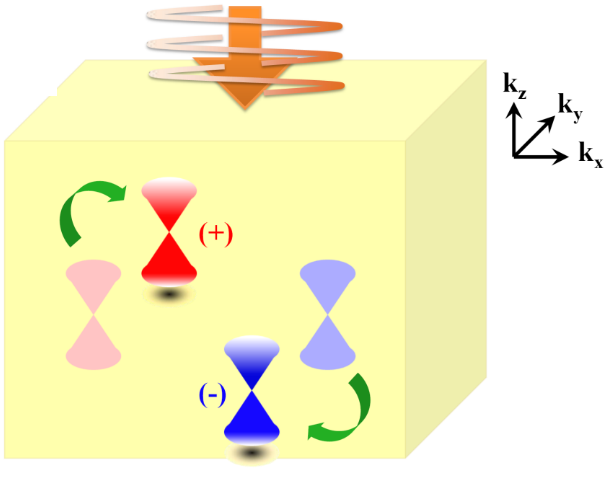

16

Weyl fermion – 3D band touching points

Why is 3D special?

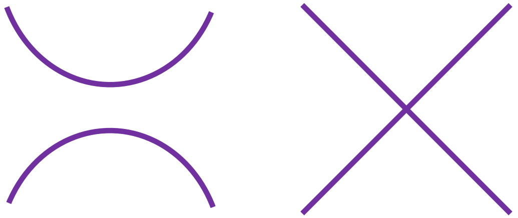

Any 2-band Hamiltonian: $$H = f_0 I_2 + \sum_{i=x,y,z} f_i(\vec{k})\sigma_i = \begin{pmatrix} f_0 + f_z & f_x - i f_y \\ f_x + i f_y & f_0 + f_z \end{pmatrix}$$

Band touching (points) iff $$f_x(\vec{k_0}) = f_y(\vec{k_0}) = f_z(\vec{k_0}) = 0$$

In 3D, conditions generically satisfied ***without fine tuning***

$\longrightarrow$ **robust against perturbation**

In 2D, additional symmetries required to force, say f_z (k) = 0 (e.g. graphene)

$\longrightarrow$ **not robust if one of those symmetries is removed**

Weyl semimetals: 3D Chiral fermion

Features:

- 3D linearly band touching points

- Come in a pair of opposite chirality
(Nielsen-Nynomiya theorem)

- Monopole and anti-monopole of Berry curvature in momentum space

$$\Omega_{\pm}(\vec{k}) = \mp \frac{\hat{k}}{2k^2}$$

- Fermi arc surface states

- Chiral anomaly

- Can be created by breaking TR or I symmetry of 3D Dirac semimetals

Berry curvature of TaAs

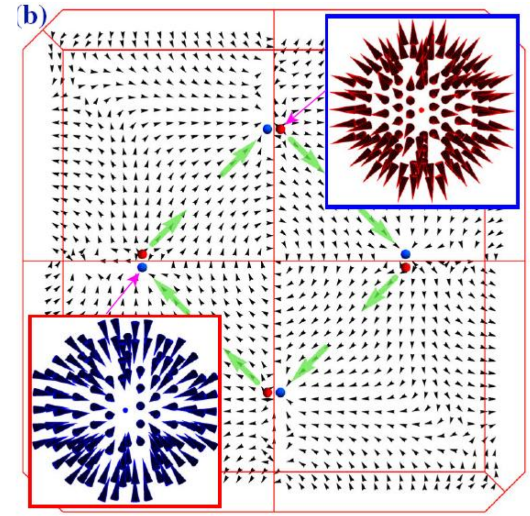

(H. Weng, et. al., PRX, 2015)

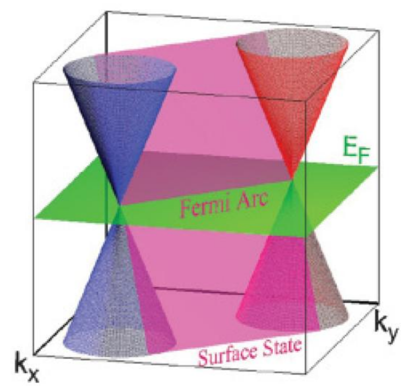

(X. Wan, et. al., PRB, 2011)

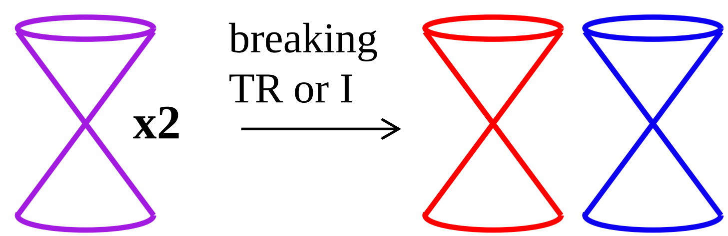

3D Dirac with both TR and I

3D Weyl

Effects of chiral photons on Dirac and Weyl fermions

2D Dirac (TR required):

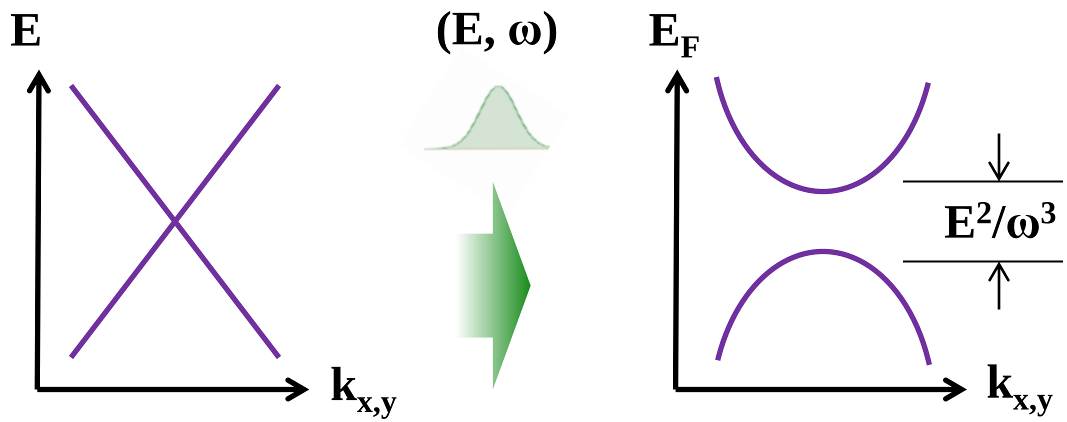

Anomalous Hall Effect!

3D Weyl (TR not required):

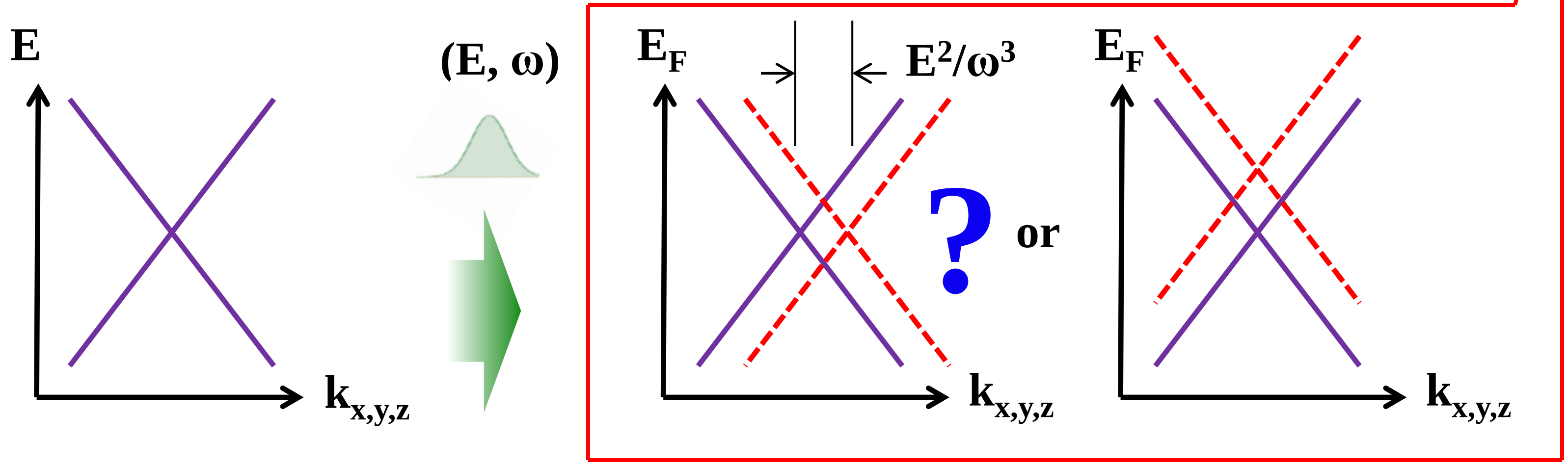

Anomalous Hall Effect in Weyl semimetals

View as a stack of 2D layers with well-defined topological invariant and σ_{xy}

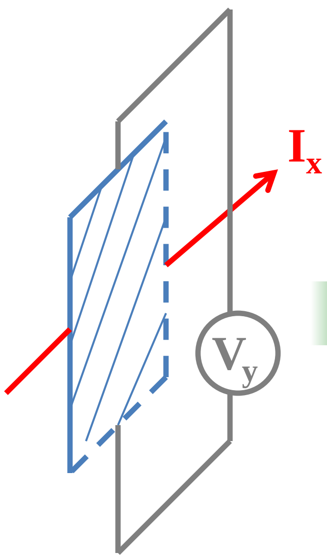

$\sigma_{xy} = Ce^2/h$

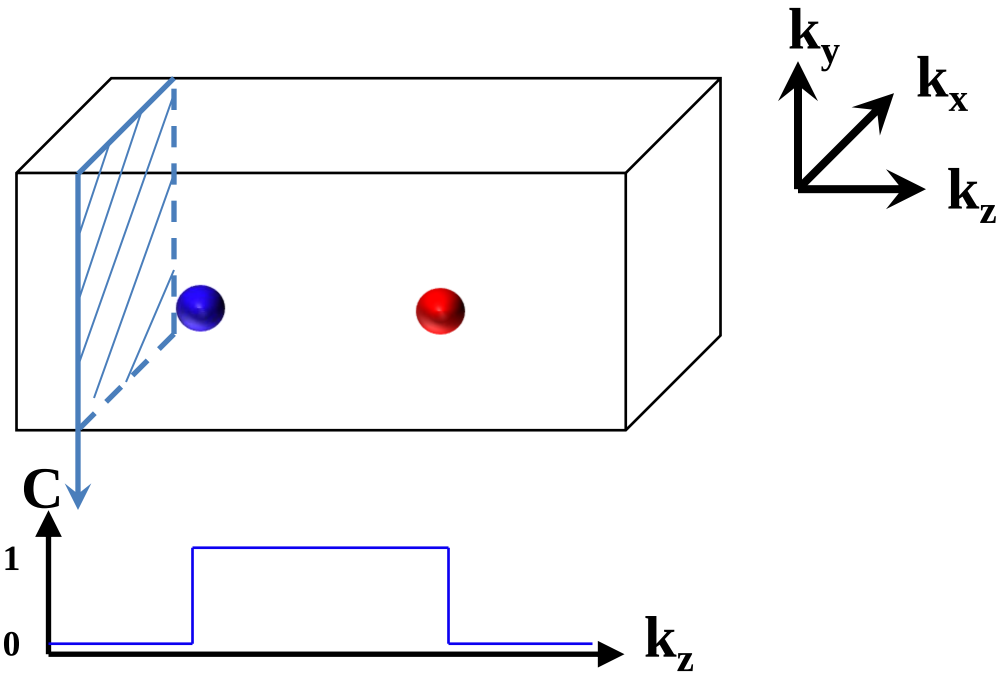

$$\boxed{\sigma_{xy} = \frac{e^2}{2\pi h}\Delta K_z}$$

(Yang, Lu and Ran, PRB, 2011)

In general, $\delta\sigma_{ij} = \frac{e^2}{2\pi h}\epsilon_{ijk}\delta\nu_k$ **with Chern vector** $\delta\nu_k = \sum_I \chi_W^{(I)} \cdot \delta q_k^{(I)}$

AHE in TR Weyl semimetals

With TR, σ_{xy} from TR Weyl pairs cancel each other

No AHE in TR Weyl semimetal!

Without drive

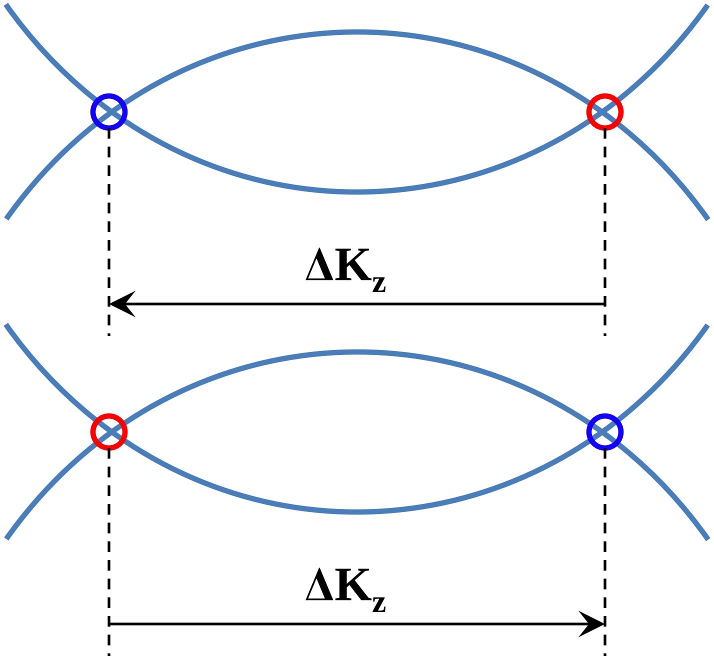

$$\sigma_{xy}/\sigma_0 = (\Delta K_z) + (-\Delta K_z) = 0$$

AHE in driven TR Weyl semimetals

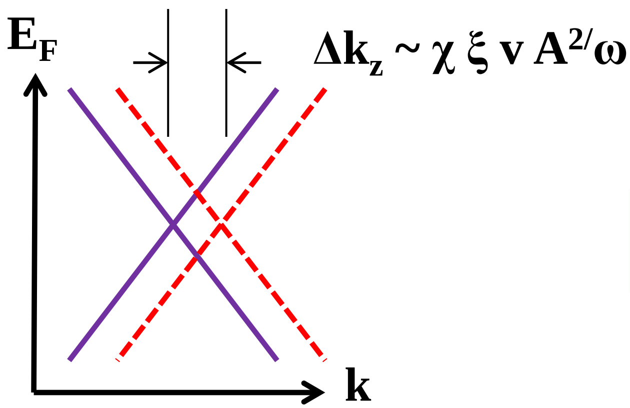

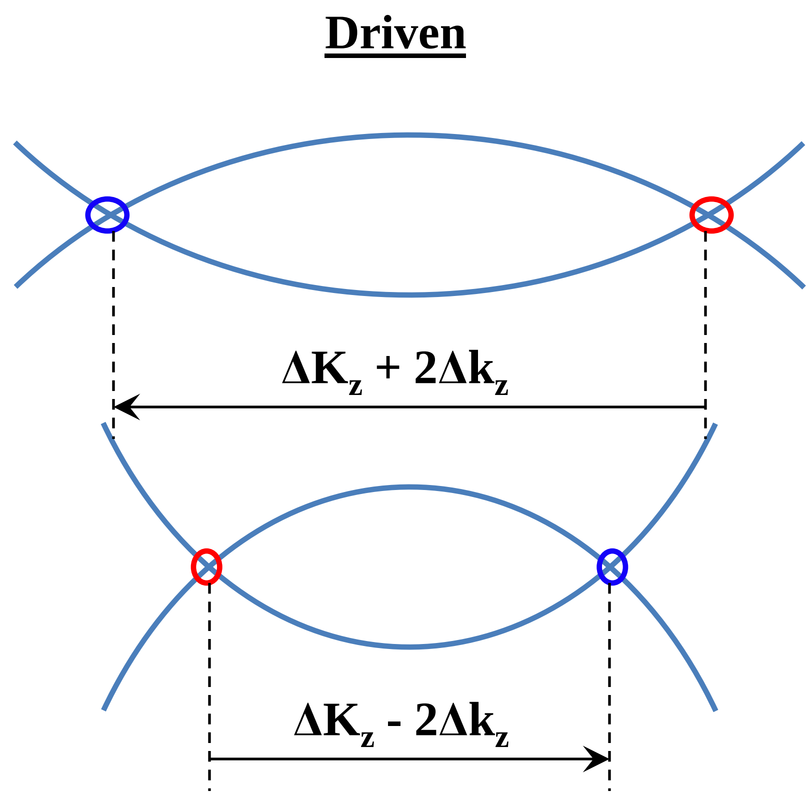

Photoinduced Weyl nodes shift
in a chirality (χ) and polarization (ξ) dependent manner

Lead to photoinduced AHE

$$\sigma_{xy}/\, \sigma_0 \sim 4\, \xi\, v\, A^2/\, \omega$$

$$\boxed{\delta\nu_z = \sum_I \chi_W^{(I)} \cdot \delta q_z^{(I)} \approx (no.\ of\ nodes)\xi v A^2/\omega}$$

(CKC, et. al., PRL, 2016)

Chirality-dependent Weyl node shift

Low-energy Weyl Hamiltonian coupled to AC drive propagating along z:

$$H_w = v\ k_i \cdot \sigma_i \qquad \vec{k} \to \vec{k} + A(\cos\omega t,\ \xi \sin\omega t,\ 0)$$

Effective Floquet contribution:

$$\Delta H_F \approx \frac{1}{\omega}[H_{-1},\ H_1] = -\left(\frac{\xi v^2 A^2}{\omega}\right)\sigma_z$$

$$\boxed{k_z \to k_z - \frac{\xi v A^2}{\omega} \ \text{ or } \ k_z - \frac{\chi \xi |v| A^2}{\omega}}$$

chirality: $\chi = \dfrac{v}{|v|}$

Anisotropy: $H_W(\vec{q}) = q_i \alpha_i \sigma_0 + q_i \beta_{ij} \sigma_j$

Coupling to higher bands: $H_{\text{lin}}(\vec{q}) = \begin{pmatrix} H_W(\vec{q}) & q_i C_i \\ q_i C_i^\dagger & D_0 + q_i D_i \end{pmatrix}$

Lattice model study

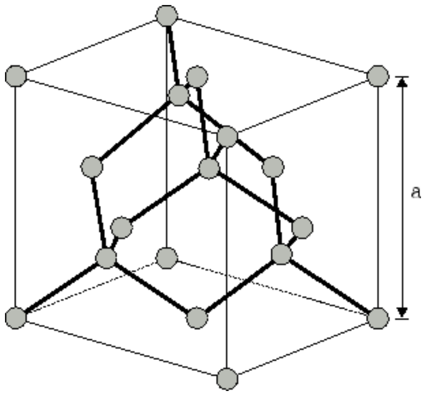

Lattice structure

Hoping model on diamond lattice that breaks inversion symmetry

$$H = -\sum_{\langle i,j\rangle}(t\, c_i^\dagger c_j + \mathrm{H.c}) + \sum_i E_i\, c_i^\dagger c_i$$
$$+ i\lambda \sum_{\langle\langle i,j\rangle\rangle}(c_i^\dagger \mathbf{e}_{ij}\cdot \mathbf{s}\, c_j - \mathrm{H.c}).$$

Supports 12 Weyl nodes (6 +ve and 6 -ve)

$$k_0 = 2\sin^{-1}\left(\frac{\epsilon}{4\lambda}\right) < \pi$$

$$\boxed{\begin{array}{ll} \vec{k}_{W-}^{(1,2)} = (\pm k_0, 0, 2\pi), & \vec{k}_{W+}^{(3,4)} = (0, \pm k_0, 2\pi), \\ \vec{k}_{W+}^{(5,6)} = (\pm k_0, 2\pi, 0), & \vec{k}_{W-}^{(7,8)} = (2\pi, \pm k_0, 0), \\ \vec{k}_{W-}^{(9,10)} = (0, 2\pi, \pm k_0), & \vec{k}_{W+}^{(11,12)} = (2\pi, 0, \pm k_0), \end{array}}$$

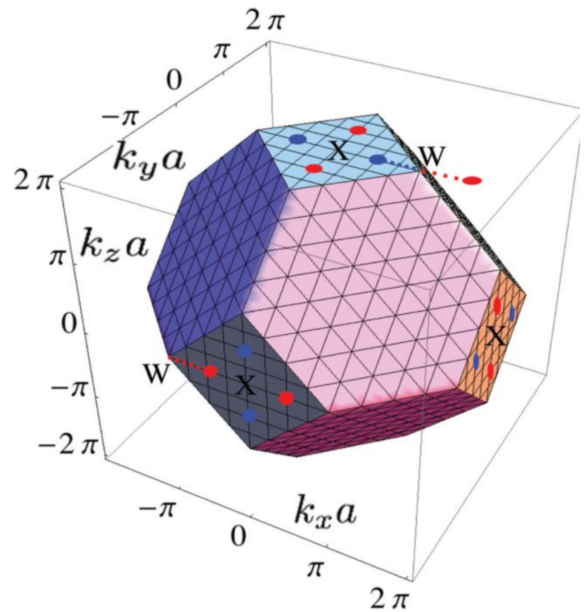

(Ojanen, PRB, 2013)

Lattice model study

Model Hamiltonian

(periodic drive)

Floquet Hamiltonian

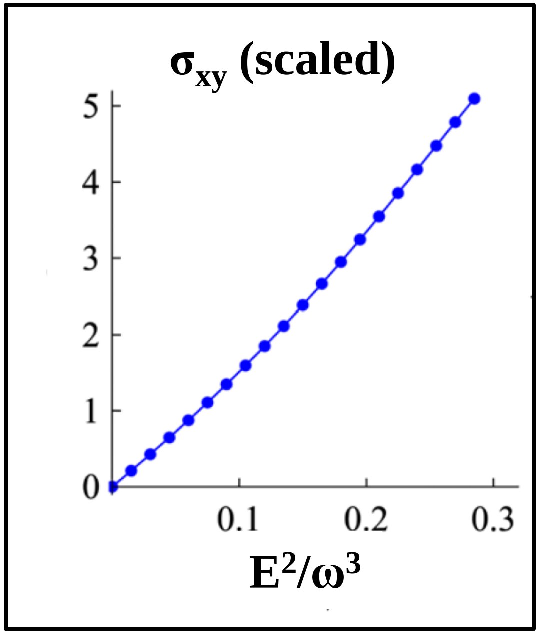

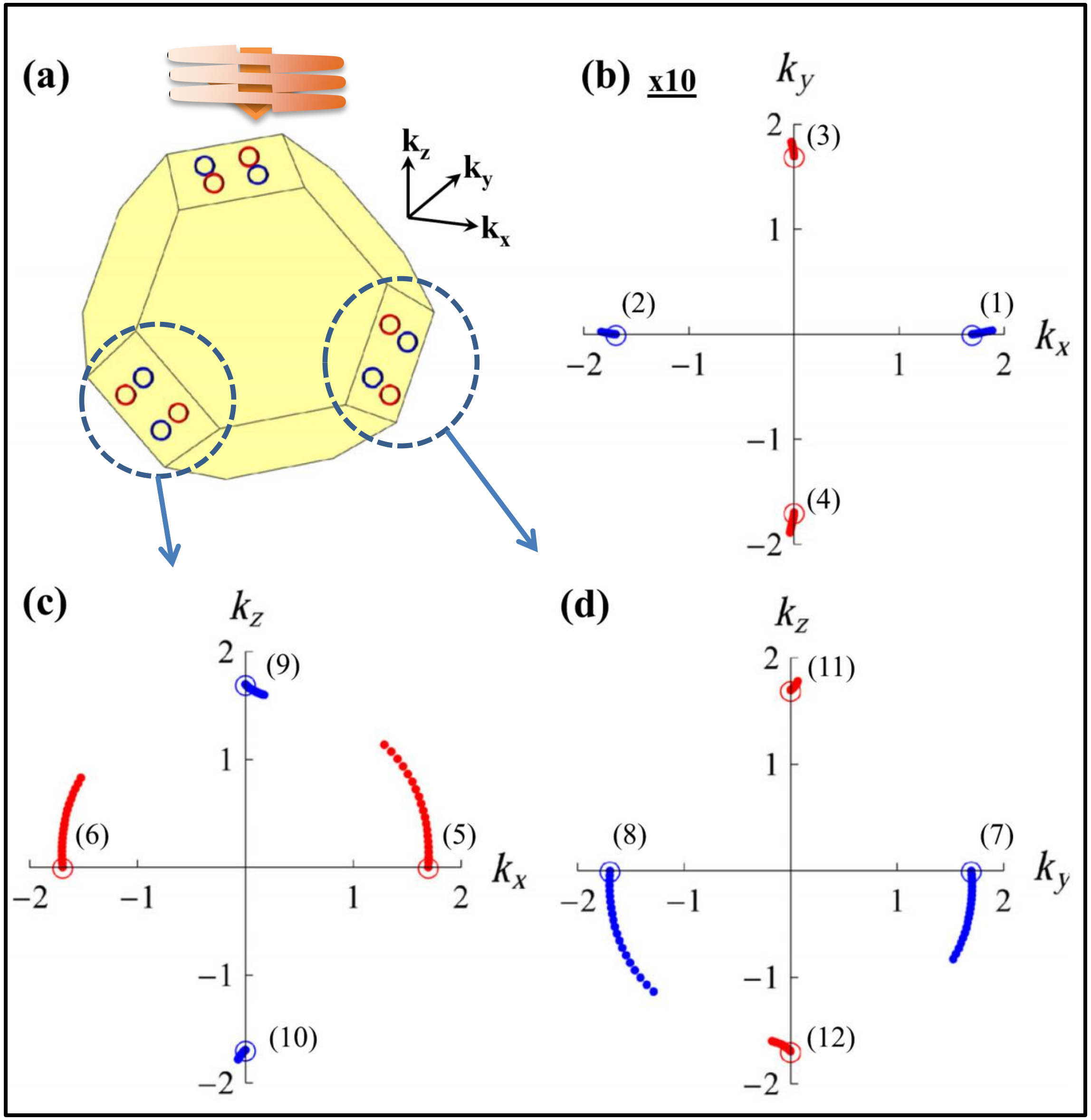

(CKC, et. al., PRL, 2016)

Effects of doping

$$\Omega_{\pm}(\vec{k}) \sim \mp \frac{\vec{k}}{2k^3}$$

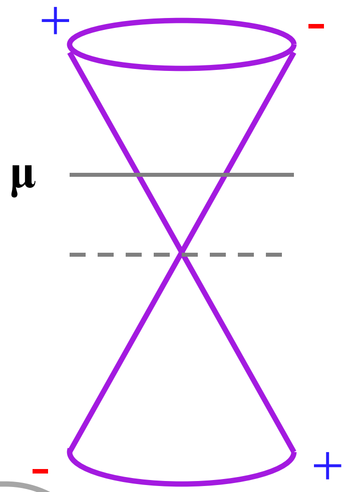

Doping only leads to negligible correction ~O(μ²)

$$\delta\sigma_{xy}(\mu) \sim \frac{e^2}{4\pi^2 h} \int_{0\le k\le k_F} d^3k\Omega(\vec{k}) \cdot \hat{k}_z \sim O(\mu^2)$$

In sensitive to node positions:

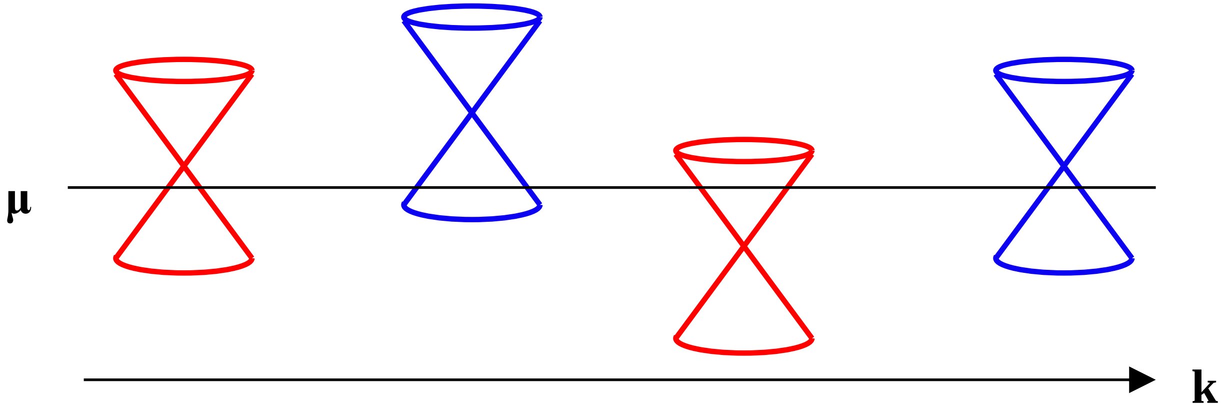

(H. Weng, et. al., PRX, 2015)

Experimental estimation on TaAs family

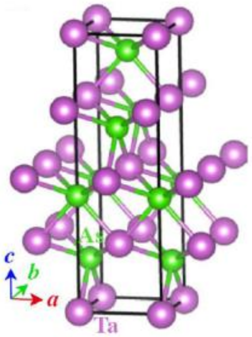

Weyl family of nonmagnetic material: TaAs, TaP, NbAs and NbP

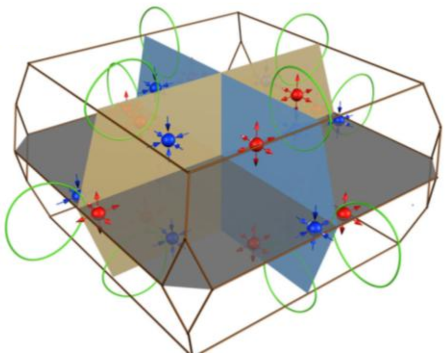

24 Weyl nodes

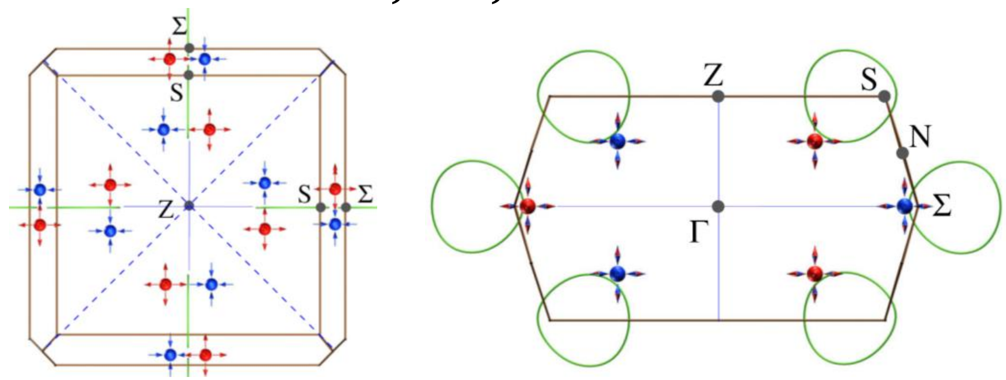

Mirror and TR symmetry

<u>CW drive</u>

- **Sample size: 100µm x 100µm x 100 nm**
- **CO_2-laser: ħω = 120meV, P = 1W**
- **Average Fermi velocity: 2 eVÅ**
- **Hall current: 1A**

V_H~ 130 nV

<u>Pulsed drive</u> **Faraday angle:** $\theta_F \sim \frac{2\alpha}{n_0 + n_s}\frac{\sigma_{xy}(0)}{\sigma_0}$ **~ 200 mrad (Weyl semimetal)**

compared to : **~ 7 mrad (graphene)**

Can we do more?

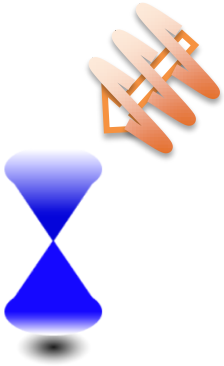

Two types of Weyl cones

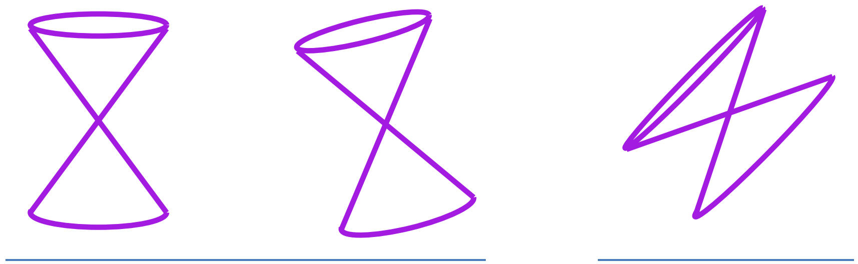

Type-I

Type-II

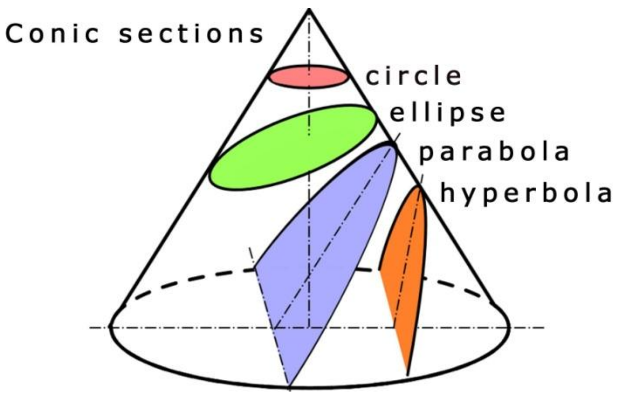

Conic section
Fermi surfaces

Type-II Weyl features:

-Open Fermi surfaces

-Finite electronic DOS

-Fermi arc surfaces states

- Anisotropic chiral anomaly

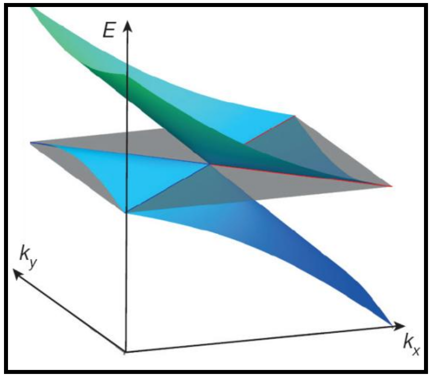

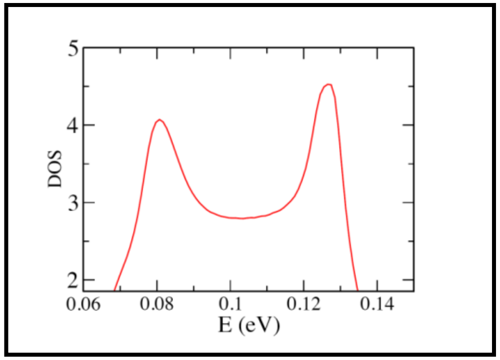

(A. A. Soluyanov, et. al., Nature, 2015)

Photoinduced type-II Weyl transition - 1

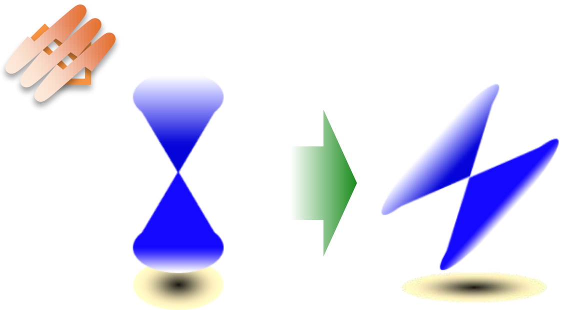

Floquet phase diagram as a function of drive amplitude (A) and angle (θ_A)

BaAuBi

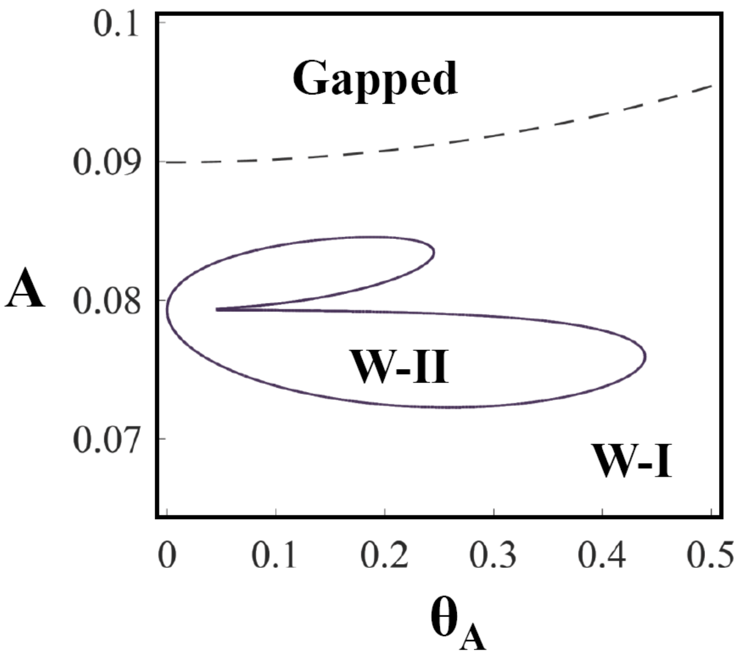

(CKC, Oh, Han and Lee, PRB, 2016)

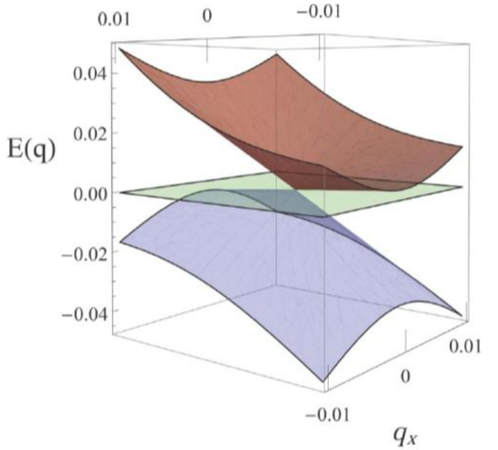

W-I

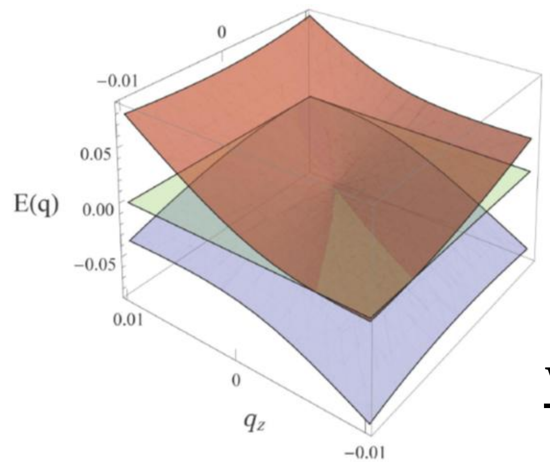

W-II

Photoinduced type-II Weyl transition - 2

<u>Linenode semimetal:</u>

- 3D linearly band touching ring

- nearly flat drum-like surface state

- interesting Berry phase features

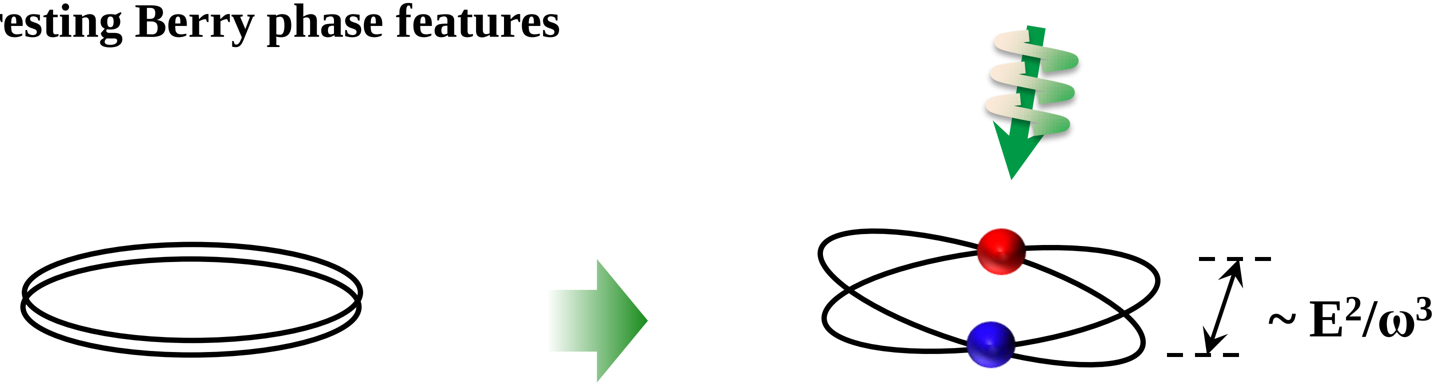

Before drive
Linenode semimetal

Driven
Weyl semimetal (type I or II)

(CKC, Oh, Han and Lee, PRB, 2016)

Topological semimetal transitions *by light!*

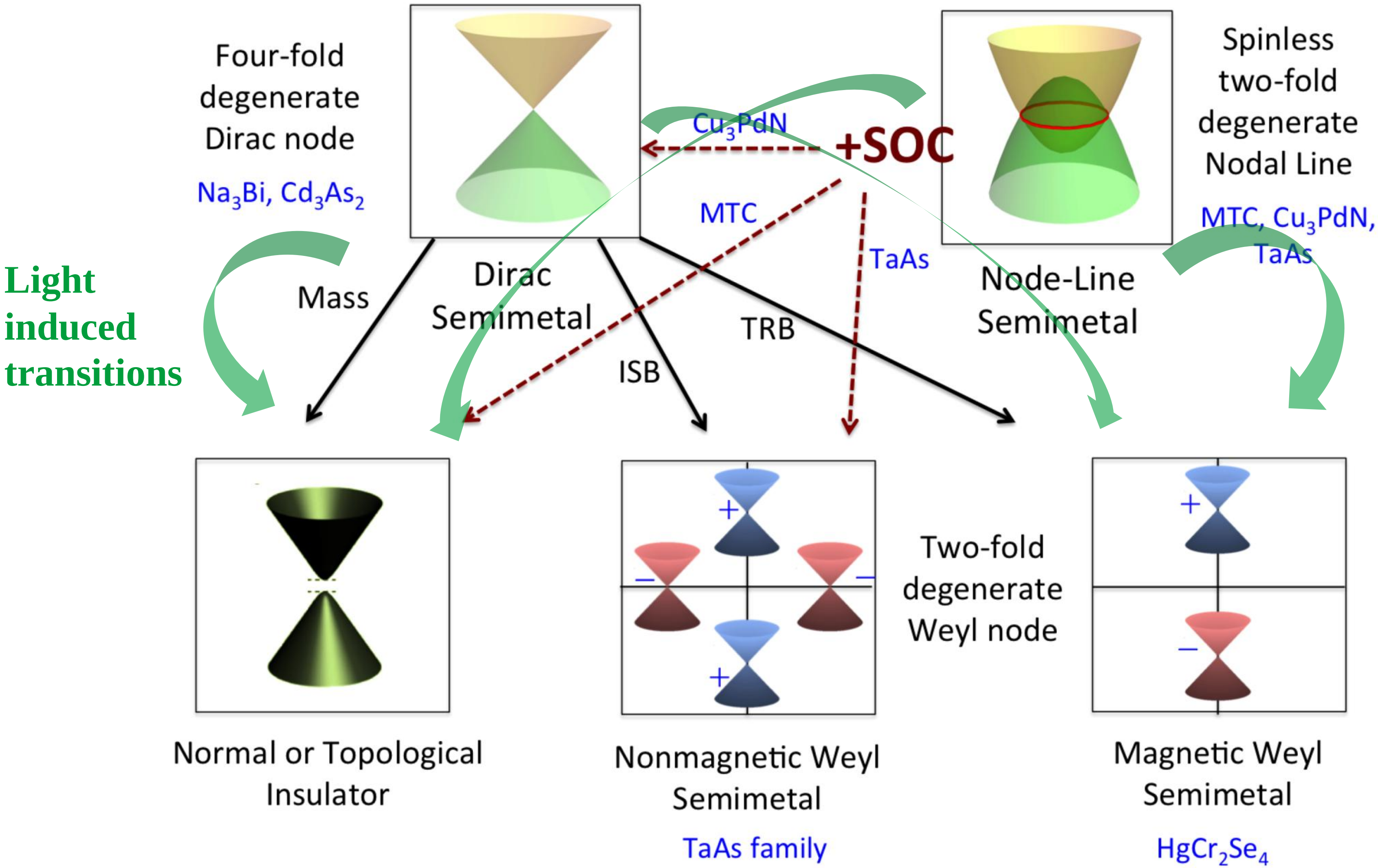

(Weng, Dai, Fang, JPCM, 2016)

Summary

➢ **Driving Weyl semimetals photoinduce anomalous Hall effect (large effect, measurable by optical and transport experiments)**

➢ **Various ways to photoinduce Weyl transitions (changes of Fermi surfaces, surfaces states, transport properties…)**

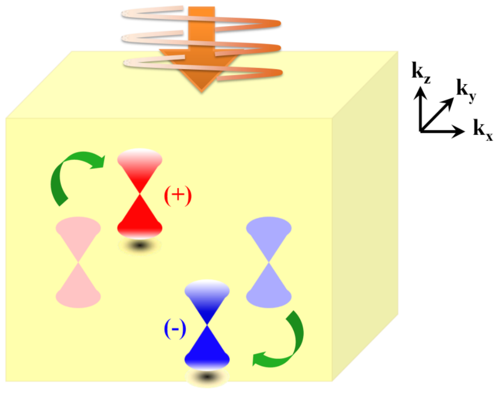

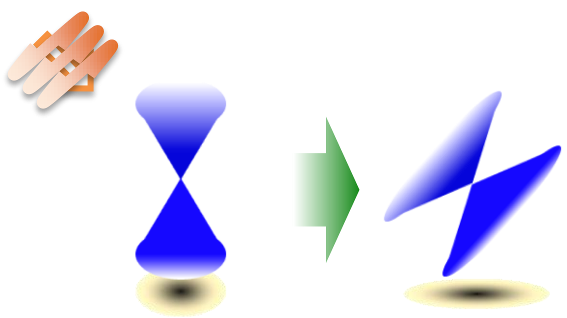

Photocurrents in Weyl semimetals

- **Circular photogalvanic effect (CPGE)**
- **Weyl semimetals as infrared detector**

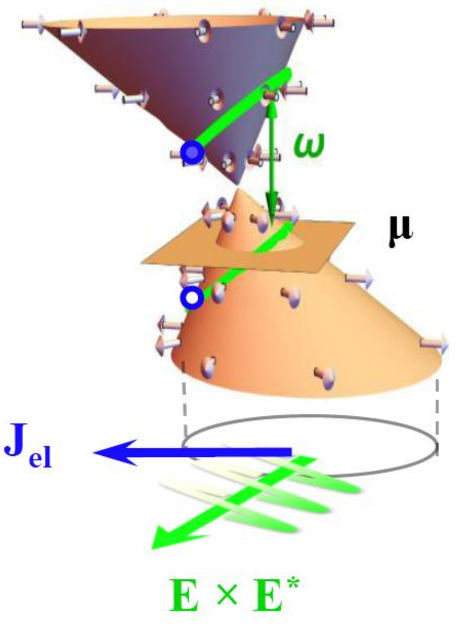

Growing interests in nonlinear photovoltaic effects

Intraband effects

-Gyrotropic magnetic: Moore and Orenstein, PRL (2010); Zhong, Orenstein and Moore, PRL (2015)
-Quantum nonlinear Hall: Sodemann and Fu, PRL (2015)
-Photovoltaic chiral magnetic: Taguchi, et. al, PRB (2016)
-Emergent electromagnetic induction: Ishizuka, et. al, PRL (2016)
-Photoinduced anomalous Hall: Chan, et. al, PRL (2016)

Interband Circular Photogalvanic effect (CPGE)

- **Quantum wells:** Ganichev, et. al, Physica E (2001)
- **Nanotubes:** Ivchenko and Spivak, PRB (2003)
- **Noncentrosymmetric media:** Deyo, et. al, arXiv:0904.1917 (2009)

- **Weyl semimetals:**

  -Konig, et.al, PRB (2017)
  -Golub, el. al, JETP (2017)
  -de Juan, et. al, Nature Comm (2017)

Infrared photodetection in various systems

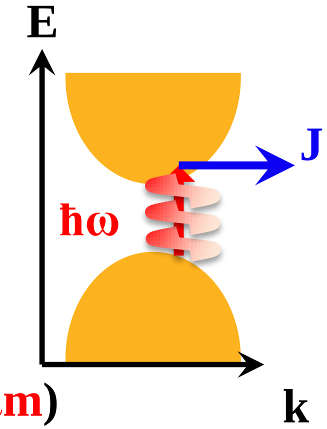

Conventional semiconductors:

- High efficiency
- But, frequency range is limited by electronic bandgap (~300meV or 4μm)

* Blackbody object at 300K has radiation peak ~73meV or 17 μm

Graphene:

- No frequency limitation (in theory)
- Very low efficiency
  as low as ~0.00001 for infrared detection

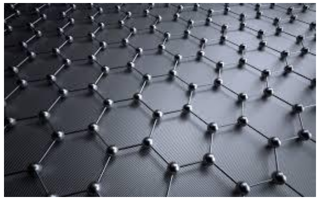

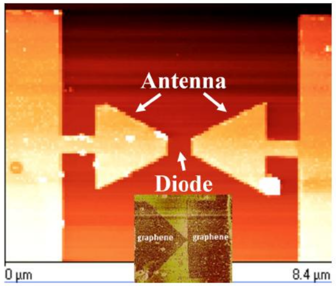

(Zhu, et al, IEEE J Quant. Electron, 2014)

3D TI (surface state) + magnetic superlattice:

- Improved efficiency
- Require external coupling

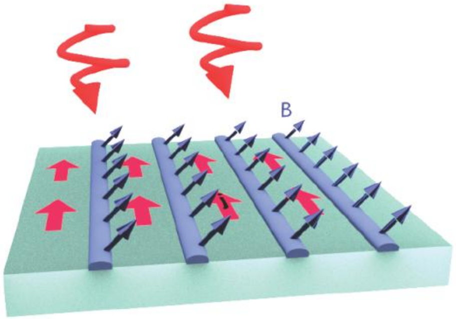

(Lindner, et. al, arXiv: 1403.0010)

Circular photovoltaic effects in Dirac and Weyl systems

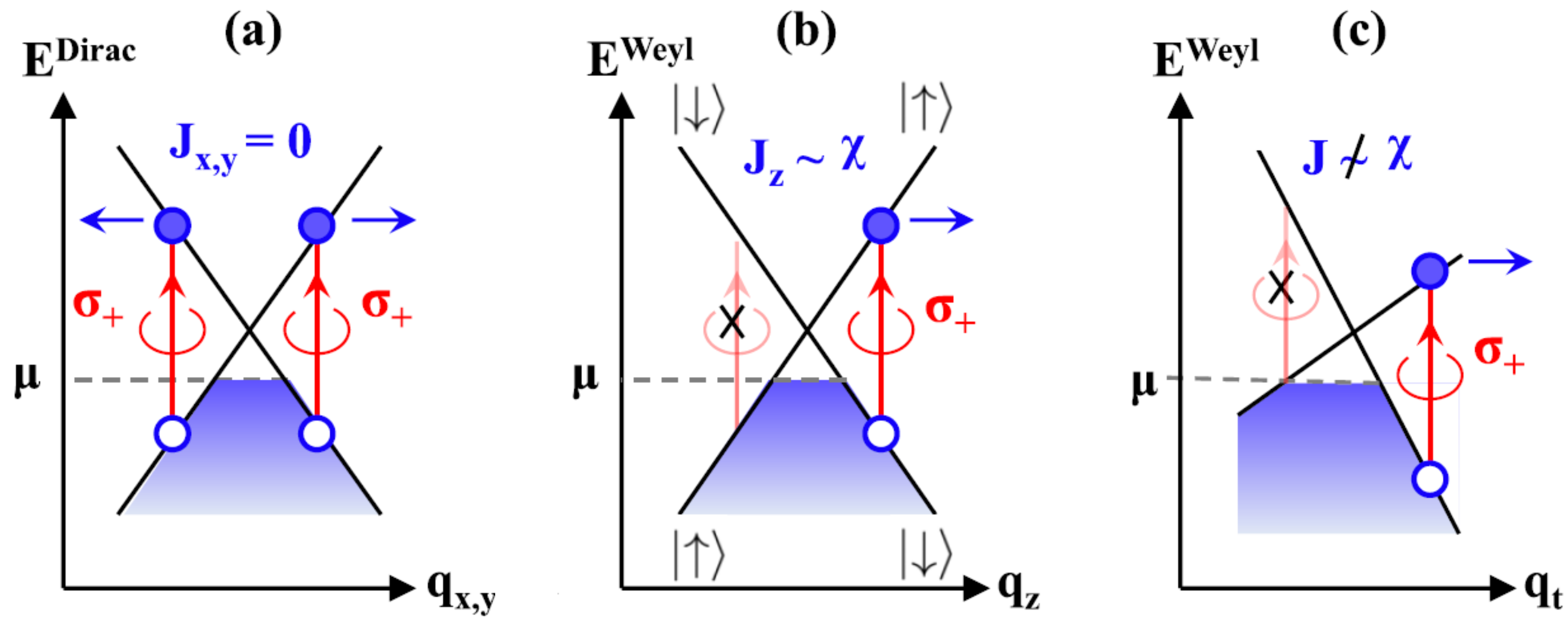

<u>**2D Dirac system**</u>

-Symmetric photoexcitation leads to zero current
- Inversion symmetry forbids current

<u>**3D Weyl system**</u>

-Asymmetric photoexcitation

- Current direction governed by chirality
➢ No net current ?

<u>**3D Weyl system (with tilt)**</u>

-Asymmetric excitation by Pauli blockade

- Current direction can be arbitrary
➢ Net current in general

Centrosymmetry vs Non-centrosymmetry

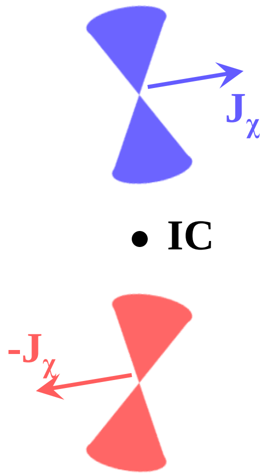

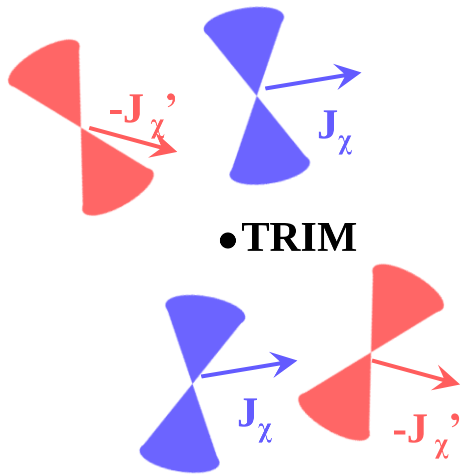

Centrosymmetric Weyl semimetal

Currents from positive and negative Weyl nodes cancel

Non-centrosymmetric Weyl semimetal

Positive and negative Weyl nodes are not symmetry related.
No current cancellation in general.

Necessary condition - 1: Break inversion symmetry

Role of mirror symmetry

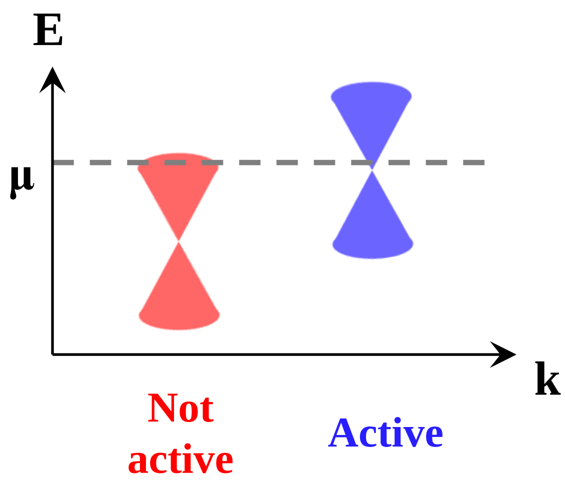

With μ imbalance, expect to see a net photocurrent.

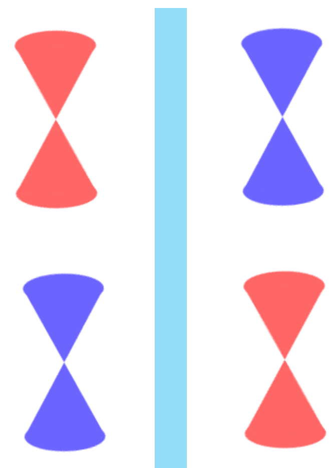

In many realistic materials (e.g. TaAs), the presence of mirror symmetry aligns the crossing points.

Still have a non-zero photocurrent?

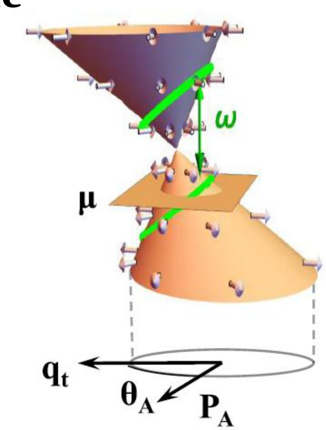

Necessary condition - 2: Finite tilts of Weyl spectra

Single Weyl node consideration

Single Weyl Hamiltonian: **tilt velocity** **Fermi velocity**

$$H_W(\vec{q}) = \hbar v_t \underline{q_t} \sigma_0 + \hbar \underline{v_F \hat{v}_{i,j}} q_i \sigma_j$$

tilt direction **Chirality χ = Sgn{Det[v_F v_{ij}]}**

Consider $v_t \rightarrow -v_t$ **and** $\hat{v}_{i,j} \rightarrow -\hat{v}_{i,j}$ **(=** $\vec{q} \rightarrow -\vec{q}$ **),**

$\Rightarrow J_i \rightarrow -J_i \Leftrightarrow$ **(J = 0 in inversion symmetric system)**

In general,

$$\vec{J}\left(\frac{v_t}{|v_t|}, \chi\right) = \frac{v_t}{|v_t|} \times \vec{J}_0 + \chi \times \vec{J}_\chi$$

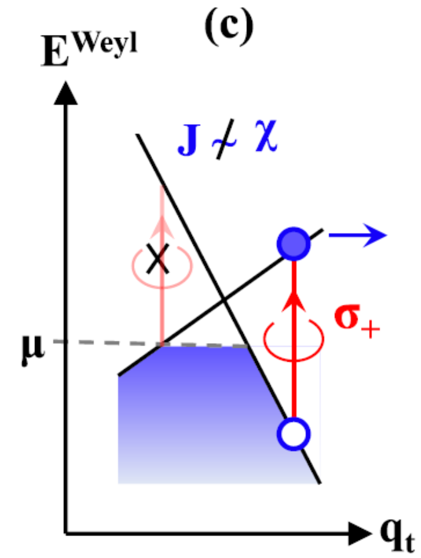

Minimal model of 4 Weyl nodes with TR symmetry

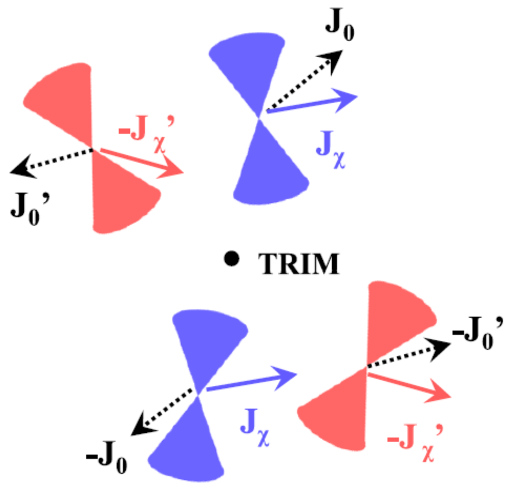

$\mathbf{J} = 2(\vec{J}_\chi - \vec{J}_\chi')$

Example plot of photocurrent generated by 4 Weyl nodes driven along some direction

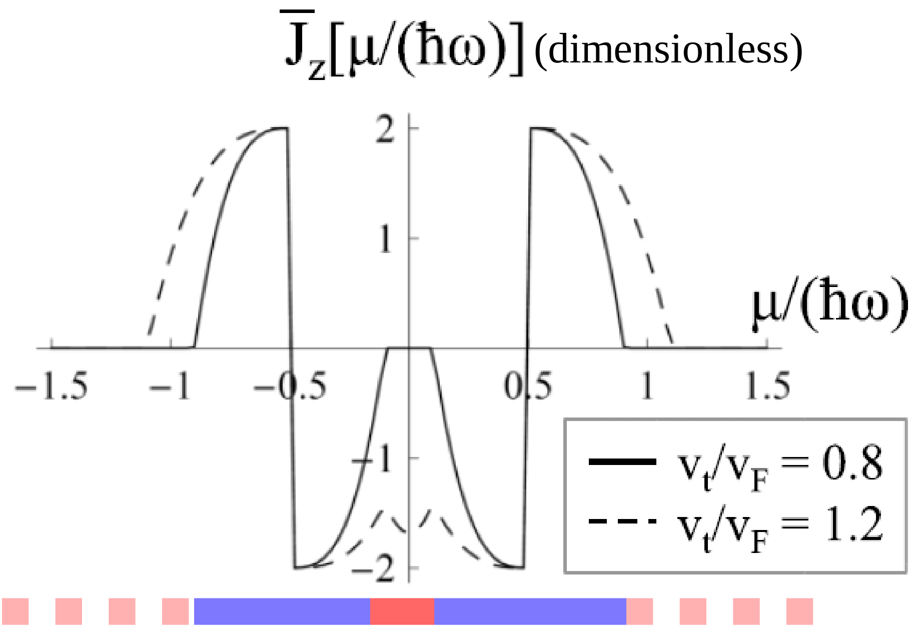

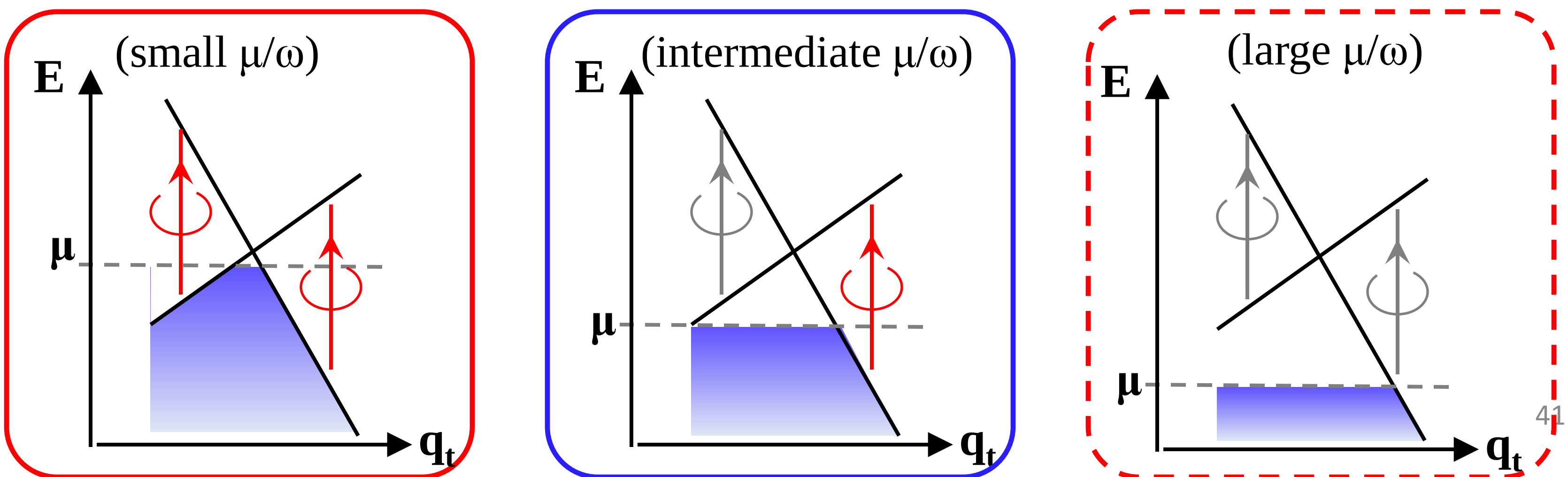

Type I vs type II Weyl cone

-Larger tilt increases the "active" region (μ/ħω)

-Magnitude of photocurrent is insensitive to tilt

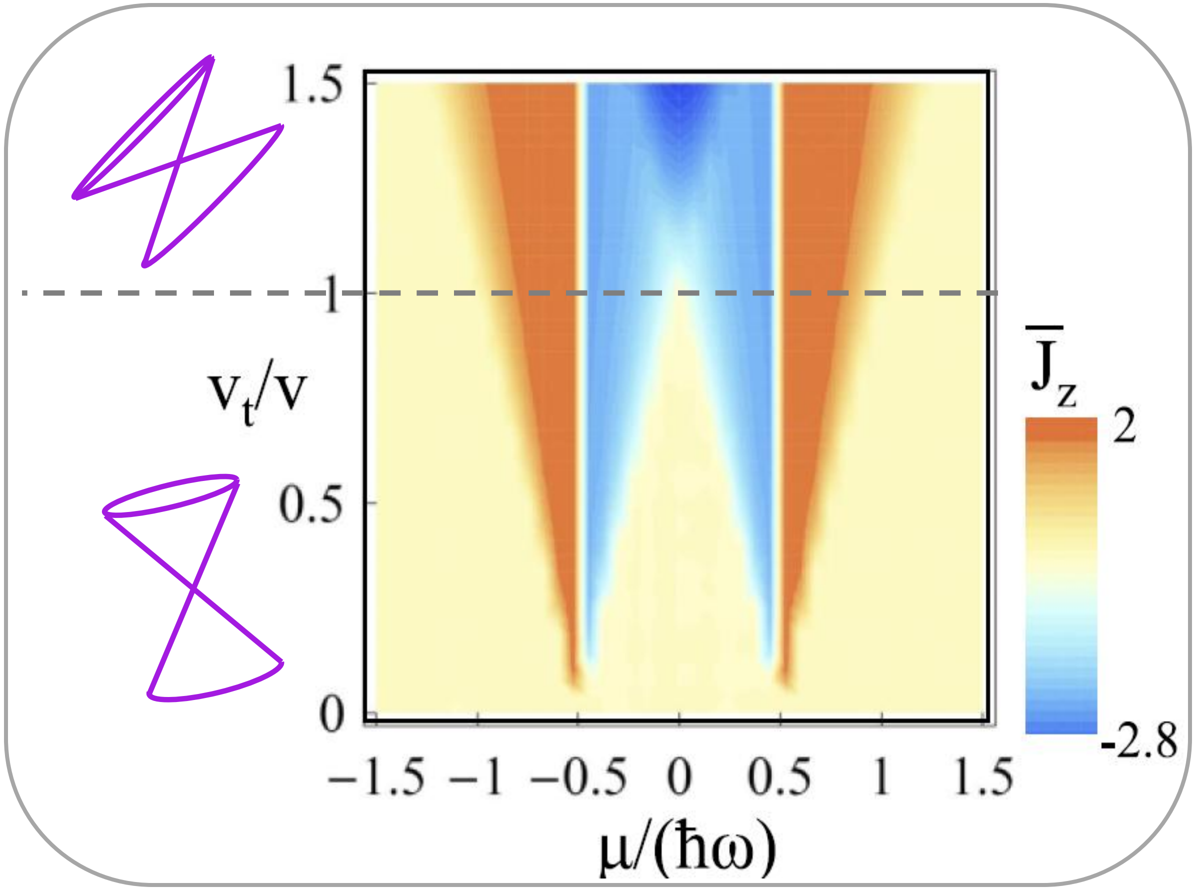

Some notable features

- Photocurrent magnitude is independent of frequency $\vec{J} = \left(\frac{e^3 \tau I}{16\pi^2 \hbar^2 \epsilon_0 c} \right) \vec{\bar{J}}$

- Photocurrent magnitude is independent of Fermi velocity (v_F)

- Photocurrent direction is determined by lattice crystal symmetry

$$J_\alpha(\omega = 0) \; = \; \eta_{\alpha\beta\gamma}(\omega, -\omega) E_\beta(\omega) E^*_\gamma(\omega)$$

Room temperature IR photodetector

Weyl semimetal candidate: TaAs
Long relaxation time ~ 45ps
Tilt ~ 60%
μ ~ 20meV

+

CO_2 laser: ħω = 120meV
Intensity: I ~ 10^6 Wm^{-2}

➢ **Current density ~ 4 x 10^7 Am^{-2} at low temperature**

- Gigantic photocurrent density can be generally induced in Weyl semimetals
- Several orders of efficiency improvement when compared to graphene on substrates

(CKC, Lindner, Refael and Lee, PRB, 2017)

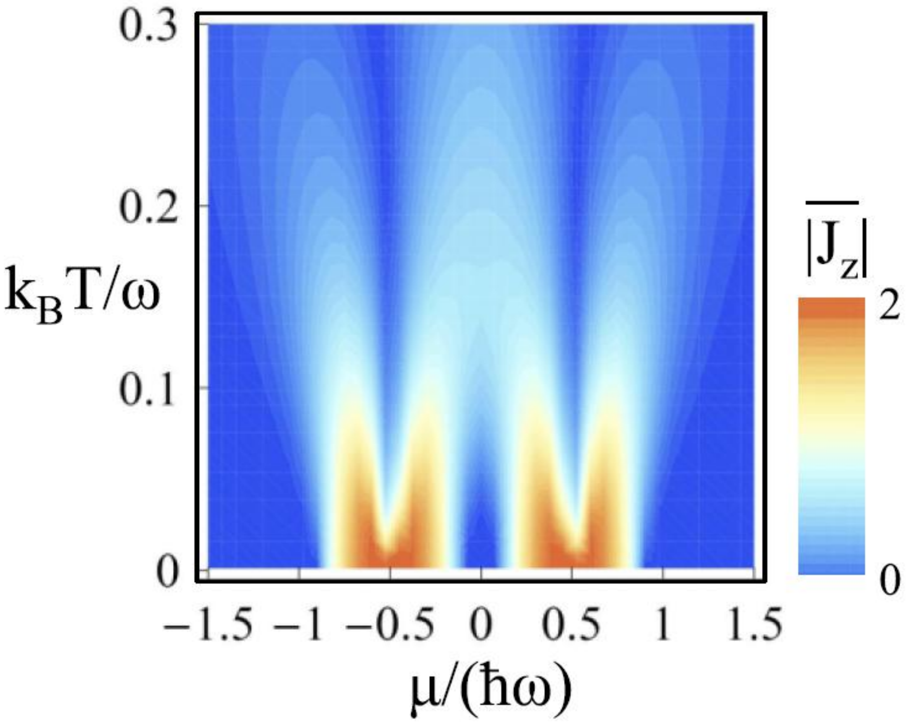

Room temperature reduction: ~ 30

Observation of circular photogalvanic effect in TaAs

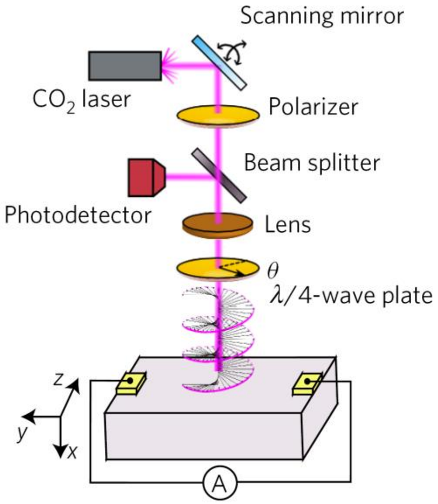

Setup:

-CO_2 laser ħω = 120meV

-TaAs Weyl dispersion tilting~ 72% and μ ~ 18meV

Observation of sizeable photocurrent amplitude ~ 40 nA.

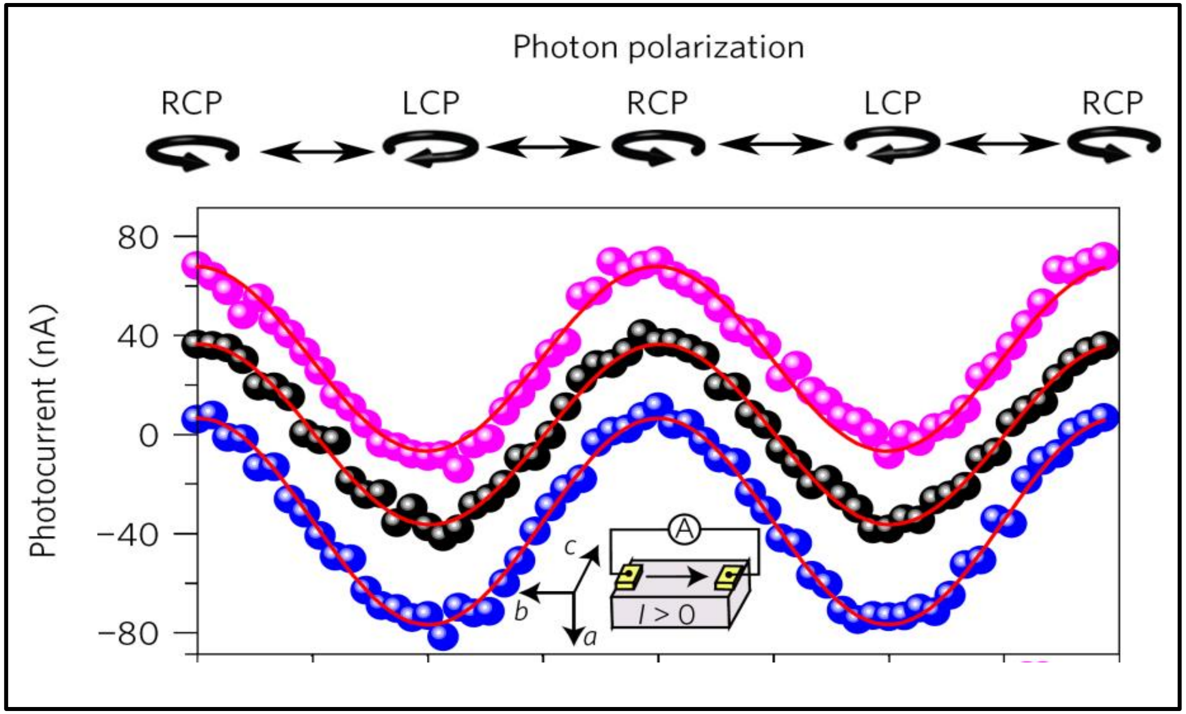

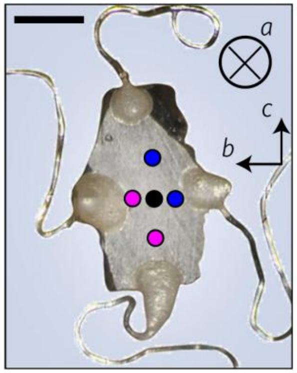

(Ma, Xu, CKC, et. al., Nature Physics, 2017)

Observation of circular photogalvanic effect in TaAs

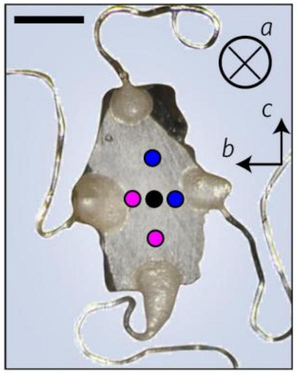

Photocurrent response tensor respects crystal symmetry

$$J_\alpha(\omega = 0) \ = \ \eta_{\alpha\beta\gamma}\, E_\beta(\omega) E^*_\gamma(\omega)$$

$$\eta_{aca} = \eta^*_{aac} = \eta_{bcb} = \eta^*_{bbc} \neq 0$$

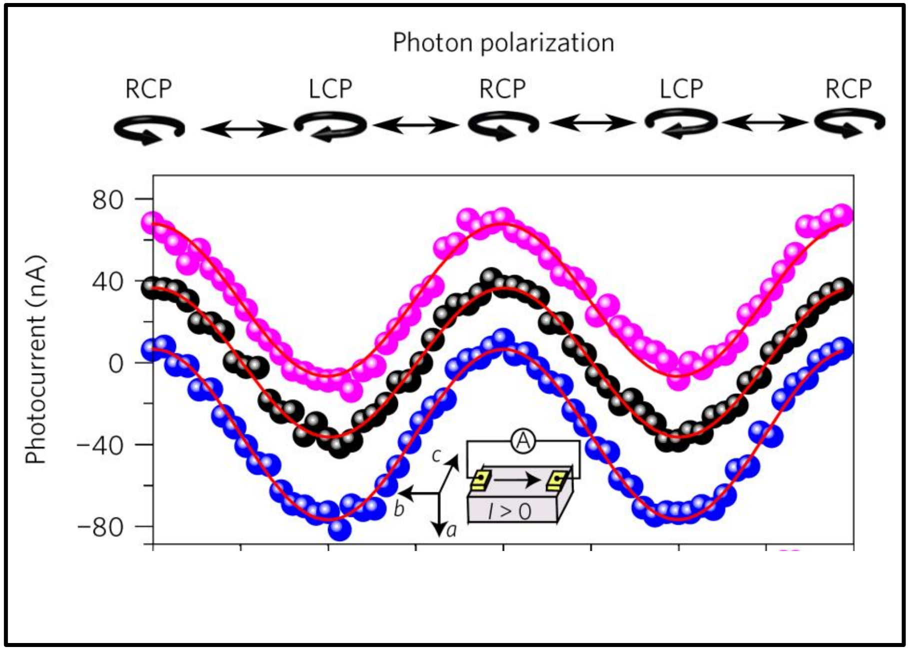

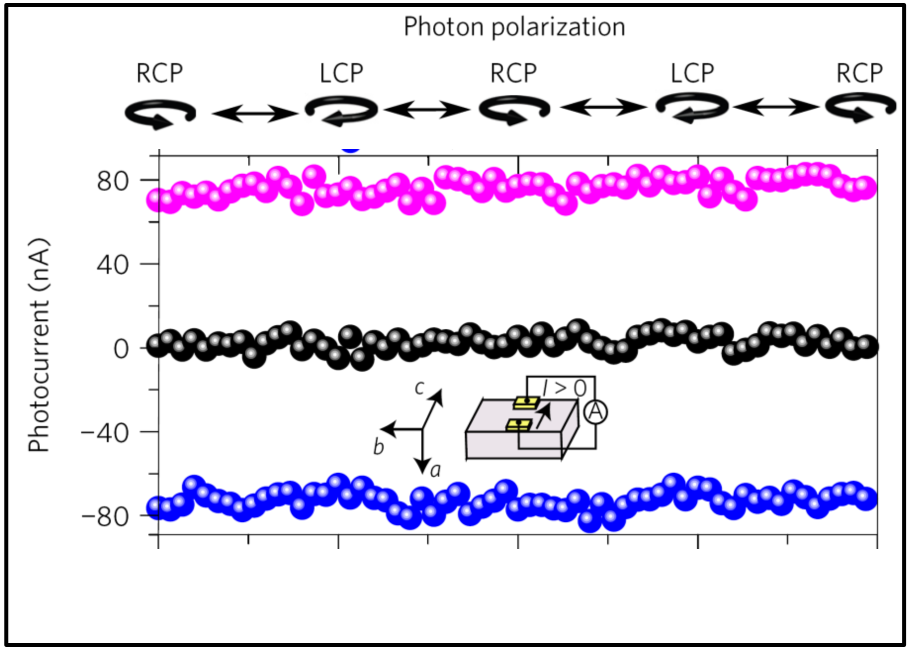

Observation of circular photogalvanic effect in TaAs

Photocurrent drops by increasing temperature due to

- reduced relaxation time

- population of excited states in Fermi-Dirac distribution

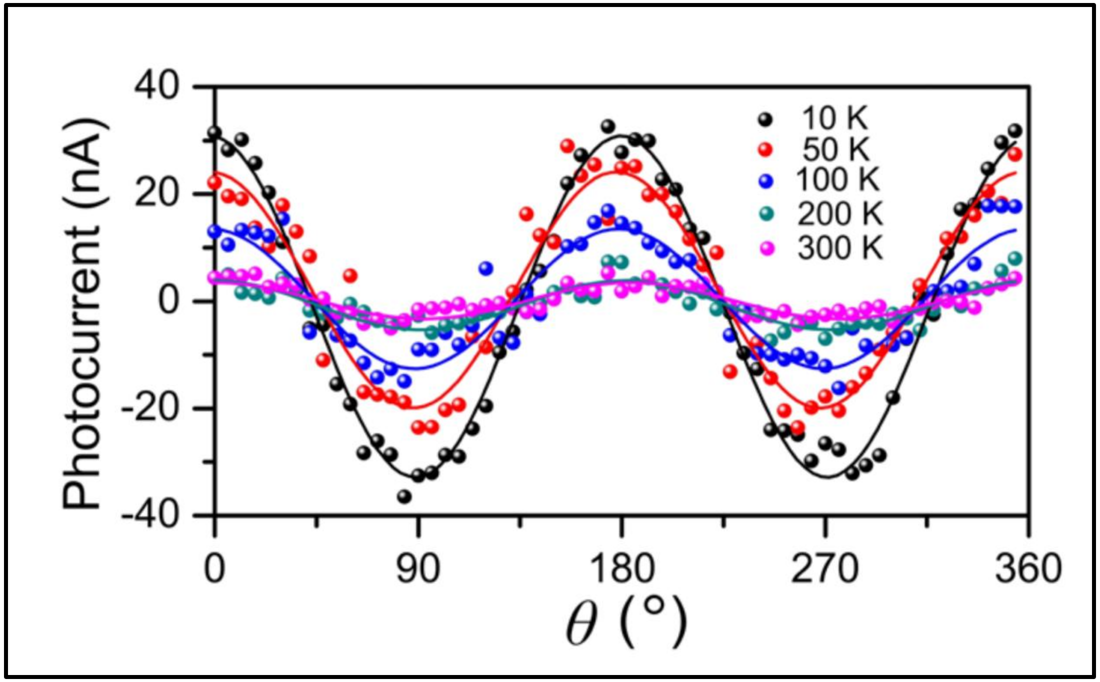

Conclusion

- Tunable Floquet-Bloch bands

Floquet band replica, open gaps by breaking TR, manipulate Weyl spectra

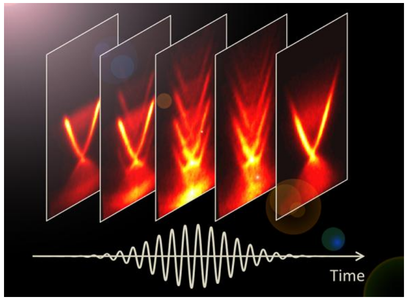

- Circular photogalvanic effect

Generic and large effect in noncentrosymmetric Weyl semimetals, promising candidate for room temperature infrared photodetector

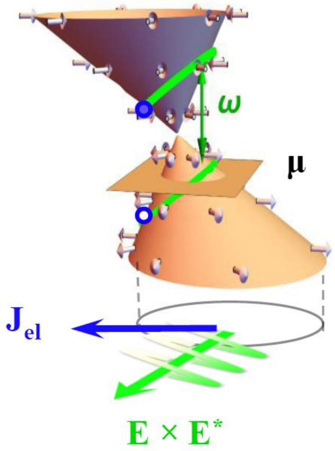

-Experimental relevance

TRARPES, photoinduced AHE, Faraday effects, photovoltaic effects, etc..